Mid-Atlantic U.S. observations of radiocarbon in CO_2: fossil and biogenic source partitioning and model evaluation

Bianca C. Baier[1], John B. Miller[1], Colm Sweeney[1], Scott Lehman[2], Chad Wolak[2], Joshua P. DiGangi[3], Yonghoon Choi[3,4], Kenneth Davis[5,6], Sha Feng[5,+], Thomas Lauvaux[5,*]

[1]NOAA Global Monitoring Laboratory, Boulder, CO 80305
[2]Institute of Arctic and Alpine Research, University of Colorado-Boulder, Boulder, CO 80309
[3]NASA Langley Research Center, Hampton, VA 23681
[4]Analytical Mechanics Associated, Hampton, VA 23666
[5]Department of Meteorology and Atmospheric Science, The Pennsylvania State University, University Park, PA 16802
[6]Earth and Environmental Systems Institute, The Pennsylvania State University, University Park, PA 16802
[+]Now at: Atmospheric, Climate and Earth Sciences Division, Pacific Northwest National Laboratory, Richland, WA 99352
[*]Now at: Groupe de Spectrométrie Moléculaire et Atmosphérique (GSMA), Université de Reims-Champagne Ardenne, UMR CNRS 7331, Reims, France 51100

Correspondence to: Bianca Baier (bianca.baier@noaa.gov)

Abstract. Accurately quantifying regional anthropogenic CO_2 fluxes is fundamental to improving our understanding of the carbon cycle and for creating effective carbon mitigation policies, and the radiocarbon to total carbon ratio in atmospheric CO_2 ($\Delta^{14}CO_2$) is a robust tracer of fossil fuel CO_2 that can discriminate between biogenic and fossil fuel CO_2 sources. NASA's Atmospheric Carbon and Transport-America (ACT-America) airborne mission between 2016 and 2019 aimed to improve the accuracy of regional greenhouse gas flux estimates, through refining understanding and characterization of fluxes and flux uncertainties in models. $\Delta^{14}CO_2$ observations from 26 flights are presented for examining seasonal CO_2 source partitioning in the Mid-Atlantic U.S. Observed variability in boundary layer CO_2 at time scales ranging from intra-day to seasonal was largely driven by biogenic CO_2 (CO_{2bio}) variability that ranged from -19.7 ppm in summer to 16.2 ppm in fall, while fossil fuel CO_2 (CO_{2ff}) variability remained at 3.3 ± 2.0 ppm. Carbonyl sulfide uptake was well-correlated with CO_{2bio} uptake, and examining this relationship, and that between CO_2 and CO_{2bio} variability reinforces the seasonal extent of gross primary productivity response throughout ACT-America. We use airborne $\Delta^{14}CO_2$ flask sampling alongside in situ carbon monoxide measurements to calculate high-frequency CO_{2ff} and evaluate the magnitude and diurnal variability of modeled CO_{2ff}, deducing likely transport errors in an example flight. Although ACT-America CO_{2ff} signals were attenuated due to broad source regions sampled, results illustrate the value of $\Delta^{14}CO_2$ sampling and observation-based methodologies for regional CO_2 flux attribution and evaluation and improvement of modeled CO_2.

1 Introduction

Anthropogenic carbon dioxide (CO_2) emissions have driven more than a 50% increase in atmospheric CO_2 abundances globally since pre-industrial levels, despite almost half of these emissions being removed from the atmosphere by terrestrial and oceanic reservoirs (i.e., "sinks"; Ballantyne et al., 2012; Friedlingstein et al., 2022). Because total CO_2 fluxes encompass biogenic,

oceanic and anthropogenic processes, and regional spatial scales are ones at which carbon mitigation strategies are generally developed and implemented, it is important that these CO_2 component processes be accurately quantified. Fossil fuel emissions represent the bulk of the net atmospheric CO_2 flux annually on regional scales for North America (King et al., 2007; USGCRP, 2018). However, while national-scale fossil fuel CO_2 fluxes for many countries are likely known to within 10% (Gregg et al.,

40   2009; Andres et al., 2012), fluxes and their variability are less certain on smaller spatial and temporal scales (USGCRP, 2018; Gurney et al., 2021). Even so, fossil fuel fluxes are currently reported with uncertainties up to five times lower than biospheric CO_2 fluxes on regional scales (Hayes et al., 2012; King et al., 2015; USGCRP, 2018).

Atmospheric CO_2 and its long-term global growth rate can be directly determined from in situ observations because observed
45   CO_2 over large land areas is a function of both fossil fuel emissions and net ecosystem exchange (NEE) with the terrestrial biosphere. Distinguishing fossil fuel from biogenic CO_2 fluxes cannot be accomplished from CO_2 observations alone (Shiga et al, 2014; Basu et al, 2016). The radiocarbon to total carbon ratio in atmospheric CO_2 (^{14}C:C, expressed as $\Delta^{14}CO_2$) has been demonstrated to be a robust and largely unbiased tracer for accurately constraining recently-emitted fossil fuel CO_2 (CO_{2ff}) into the atmosphere because fossil fuels do not contain ^{14}C (Levin et al., 2003; Levin and Karstens, 2007; Graven et al., 2009;
50   Vogel et al., 2010; Miller et al., 2012; Turnbull et al., 2006, 2011a, 2011b, 2015). By isolating this fossil fuel component and its variability relative to background levels, the remaining variability in CO_2 can be attributed to biogenic processes.

Inverse models using only CO_2 measurements can theoretically be used to disaggregate anthropogenic and biogenic CO_2 fluxes when these emissions can be adequately separated in time and space, but given the low density of most regional measurement
55   networks, fossil and biogenic fluxes are co-located, so this disaggregation cannot be achieved in practice (Shiga et al., 2014; Basu et al., 2016). In many situations from regional to global scales, prior fossil CO_2 emissions are traditionally pre-specified and not optimized in CO_2 measurement-based inversions (Gurney et al., 2003; Ciais et al., 2010; Schuh et al., 2010; Lauvaux et al., 2011) on the basis that fossil fluxes are much better known than terrestrial biospheric fluxes. Much work has been done to characterize model uncertainty and improve estimates of CO_2. At the continental scale and for annual time frames, Feng et
60   al., (2019a) used a forward calibrated model ensemble (Feng et al., 2019b) to show that the uncertainty in simulated North American atmospheric CO_2 mole fractions comes primarily from two approximately equivalent sources: fossil fuel emissions and biogenic CO_2 fluxes. At these time scales, these two sources greatly outweighed the uncertainty contributions from atmospheric transport and from continental boundary conditions, and Feng et al. (2019a) note that accurate accounting of fossil fuel emissions uncertainties in models can further improve regional biospheric flux estimates. Brophy et al. (2019) emphasized
65   the need for varying prior fossil fuel emissions estimates in time, alongside needed improvements in the representation of atmospheric transport to accurately represent CO_2 fluxes at ~sub-annual and regional scales. Modelers have also relaxed the assumption of perfectly known fossil CO_2 emissions – and have lowered fossil fuel emissions uncertainties – by assimilating $\Delta^{14}CO_2$ measurements (or CO_{2ff}) alongside CO_2 and carefully controlling systematic model errors and errors in prior flux estimates (Basu et al., 2016, 2020; Fischer et al., 2017).

Deleted: ,

Deleted: however

Deleted: any

Using aircraft $\Delta^{14}CO_2$ observations, an effort has been made to evaluate modeled CO_{2ff} and to estimate or verify regional emissions inventories (e.g. Graven et al., 2009; Basu et al., 2020). At the urban scale, studies have also successfully used $\Delta^{14}CO_2$ measurements alongside in situ carbon monoxide (CO) observations from surface- and aircraft-based platforms, to calculate high-resolution proxy estimates of recently-added fossil fuel CO_2 to the atmosphere, given well-characterized fossil fuel CO_2:CO ratios (Vogel et al., 2010; Turnbull et al., 2011a, 2019; Lauvaux et al., 2020; Wu et al., 2022). As biogenic CO_2 emissions and sinks – even within cities – are non-negligible, and ignoring these signals could potentially bias fossil fuel CO_2 emission inventories, $\Delta^{14}CO_2$ measurements play an important role in determining biogenically-driven (CO_2 photosynthesis and respiration) emissions or sinks (Levin et al., 2003; Lopez et al., 2013; Turnbull et al., 2015; Miller et al., 2020). One tracer that could aid in the understanding of CO_2 uptake processes alongside $\Delta^{14}CO_2$ is carbonyl sulfide (OCS), which is taken up by plants but not respired (Montzka et al., 2007; Campbell et al., 2008).

NASA's multi-year Atmospheric Carbon and Transport (ACT)-America Earth Venture Suborbital mission was directed toward improving the accuracy of regional greenhouse gas flux estimates, specifically through refining our understanding and implementation of CO_2 and methane (CH_4) transport, fluxes and flux uncertainties and background levels in inverse models (Davis et al., 2021). During this mission, five seasonal research flight campaigns were conducted between 2016 and 2019 for evaluation and subsequent improvement of terrestrial carbon cycle models and filling gaps in the eastern U.S. carbon monitoring network. With a strong focus on transport of carbon via weather systems, atmospheric trace gases and meteorological variables were also observed across multiple synoptic cycles, across cold and warm air sectors and from the boundary layer to the upper troposphere. While the ACT mission was not targeting large carbon emissions signals in urban areas as in the abovementioned studies, we focus on carbon flux attribution and model evaluation here. We analyze a spatially dense set of airborne whole-air flask $\Delta^{14}CO_2$ measurements collected during ACT in the Mid-Atlantic U.S. alongside those of other gas-phase species such OCS, a tracer for photosynthetic uptake of CO_2, to first distinguish between biogenically-driven and fossil fuel atmospheric CO_2 variability relative to background levels. Second, we apply the methodology of previous authors (Levin and Karstens, 2007; Vogel et al., 2010; Turnbull et al., 2011a; Maier et al., 2024a) to the broad, Mid-Atlantic U.S. region, calculating high-frequency fossil fuel CO_2 enhancements using in situ carbon monoxide (CO) observations, and investigate the utility of this technique for evaluating modeled atmospheric fossil fuel-CO_2 enhancements above background levels for an example ACT research flight along the northeastern corridor.

Deleted: strong
Deleted: for verifying
Deleted: ; Graven et al., 2018
Deleted: ,
Deleted: six-week
Deleted: as carbonyl sulfide (
Deleted:)
Deleted: and carbon monoxide (CO) to
Deleted: seasonal fossil fuel- and
Deleted: with respect
Deleted: 3
Deleted:
Deleted: transport of

2 Data and Methods

2.1 ACT-America flight campaigns

During the ACT mission, the eastern half of the coterminous U.S. was broadly surveyed by two research aircraft: the NASA Langley Beechcraft B-200 King Air and the NASA Wallops C-130 Hercules. Of the Mid-Atlantic, Midwestern and Southern U.S.-focused measurement regions, air samples for $\Delta^{14}CO_2$ measurement were collected only in the Mid-Atlantic region due to proximity to the northeastern U.S. urban corridor and likelihood for higher $\Delta^{14}CO_2$ signals. Sampling in the Mid-Atlantic region focused heavily on the extensive forests and croplands with flights capturing distant urban influence, and a selected few flights specifically targeted the urban northeastern corridor. The first ACT campaign occurred during summer 2016 (July 18th -August 28th) and is omitted from this analysis due to the absence of $\Delta^{14}CO_2$ sampling. Four subsequent ACT campaigns described here occurred during winter 2017 (March 1st-10th), fall 2017 (October 1st-15th), spring 2018 (May 4th-20th), and summer 2019 (July 7th-27th) for a total of 26 flights with atmospheric sampling for $\Delta^{14}CO_2$. Research flights were primarily conducted between 11:00 and 18:00 local time to sample a well-developed atmospheric boundary layer (ABL), through long, level-leg flight transects. Airborne atmospheric sampling during individual research flights was focused at altitudes within the ABL (flight altitudes of 330 m above ground level in most cases) where greenhouse gas abundances are strongly influenced by surface fluxes with occasional sampling in the free troposphere (FT, ~2400 to 9000 m above mean sea level (ASL)) to determine chemistry and isotopic composition of background air against which observed ABL enhancements or depletions are assumed to occur. Because a scientific goal of ACT was to improve the simulation of atmospheric transport of greenhouse gases in regional-scale inversions under real-world conditions, research flights were organized to sample across synoptic weather patterns (Pal et al. 2020). Wei et al., (2021) describe the ACT observational and numerical data products.

2.2 Whole-air sample collection and flask radiocarbon measurements

NOAA Programmable Flask Packages (PFPs) were installed on each aircraft for the collection of whole-air samples. Each PFP contains 12, 0.7 L borosilicate glass flasks and for ACT campaigns between 2017 and 2019, these automated systems were connected to a Peltier gas chiller to efficiently dry air samples to less than 1% atmospheric water vapor prior to air sample collection. Flask filling times varied between two (ABL) to four minutes (FT) depending on the altitude of the aircraft. A Programmable Compressor Package (PCP) pressurized each flask to 275 kPa yielding ~ 2 standard liters (L) of air collected per flask. Technical details of these flask sampling systems used during ACT are described in Baier et al. (2020).

For each flight day, roughly six to eighteen total flasks were filled on each aircraft platform between the altitudes of 300-9000 m ASL. The ratio of well-mixed ABL to FT flasks sampled during ACT was generally 5:1. Because approximately 2 L of sample air is required for high precision $\Delta^{14}CO_2$, in addition to the long-lived greenhouse gases (CO_2, CH_4) and other low concentration gases such as OCS and CO, two PFP flasks were filled in parallel (i.e. 'paired sampling') when sampling for

$\Delta^{14}CO_2$ measurements. Post-flight, PFPs were transferred to the NOAA Global Monitoring Laboratory and the University of Colorado/INSTAAR Stable Isotope Laboratory for measurement. The first flask of each paired sample is analyzed for greenhouse gases, OCS, and a suite of hydrocarbons, halocarbons, and stable isotope ratios ($^{13}C:^{12}C$) of CO_2 and methane using methods described in Baier et al. (2020), online (https://gml.noaa.gov/ccgg/aircraft/analysis.html) and in Vaughn et al. (2004). Remaining sample air in the first flask after these measurements is combined with the entire second, paired flask for a single $\Delta^{14}CO_2$ measurement. The University of Colorado INSTAAR Laboratory for AMS Radiocarbon Preparation and Research (NSRL) conducts the CO_2 extraction from flask sample air. Pure CO_2 is archived until near the time of $\Delta^{14}CO_2$ measurement, at which time the pure CO_2 is graphitized to pure carbon "targets" and these graphitized samples are transferred to the University of California at Irvine for high-count accelerator mass spectrometry (AMS) ^{14}C measurement (Turnbull et al., 2007; Lehman et al., 2013). In total, 380 $^{14}CO_2$ samples were analyzed throughout the ACT campaigns: 87 in winter 2017, 100 in fall 2017, 104 in spring 2018 and 89 in summer 2019.

2.3 Radiocarbon-based CO_2 partitioning

Radiocarbon (^{14}C) is produced naturally in the troposphere and stratosphere via cosmic ray-induced reactions between neutrons and atmospheric nitrogen (N_2) (Libby, 1946). Measurements are presented as $\Delta^{14}CO_2$ in units of per mil (‰), or the part per thousand deviation of the measured $^{14}C:C$ ratio from that of the international measurement standard material, after correction for mass dependent fractionation and radioactive decay since the date of collection (Stuiver and Polach, 1977). Given that the ^{14}C half-life is approximately 5730 years (Godwin, 1962), and that fossil fuel carbon has been isolated from the atmosphere for millions of years, the radiocarbon content of fossil fuels is zero and therefore $\Delta^{14}CO_{2ff}$ is -1000 ‰ on the delta (Δ) scale. Therefore, addition of fossil fuel CO_2 to the atmosphere produces a quantitative reduction in atmospheric $\Delta^{14}CO_2$ over and downwind of emissions sources. Paired observations of $\Delta^{14}CO_2$ and CO_2 in flasks sampled in the Mid-Atlantic region can thereby provide a robust method for distinguishing between terrestrial biogenic (CO_{2bio}) and fossil fuel (CO_{2ff}) CO_2 sources given a known background. The CO_2 mass balance over land is:

$$CO_{2obs} = CO_{2bg} + CO_{2ff} + CO_{2bio} \qquad (1)$$

Expanding CO_{2bio}, which results from Net Ecosystem Exchange, into a sum of photosynthetic (*photo*) and respiration (*resp*) fluxes ($CO_{2resp} + CO_{2photo}$) and adding the respective isotopic signatures ('Δ', for $\Delta^{14}CO_2$) for all terms gives Equation (2):

$$\Delta_{obs}CO_{2obs} = \Delta_{bg}CO_{2bg} + \Delta_{ff}CO_{2ff} + \Delta_{resp}CO_{2resp} + \Delta_{photo}CO_{2photo} + N^{14}C_{nuc}/R_{std}, \qquad (2)$$

where the individual budget terms are the product of the isotopic ratio and CO_2 mole fraction, which is a conserved quantity (Tans et al., 1993). Here, *obs* is the observed atmospheric mole fraction of CO_2 in the ABL and is a function of variations in

fossil fuel (*ff*) and biogenic (*bio*) CO_2 differences from a varying CO_2 background (*bg*) level. We note that, an oceanic term is sometimes written in Equation (1), but we assume that the dominant oceanic CO_2 influence is encompassed in the background (*bg*) term. Photosynthesis and respiration contributions are stated separately in the isotopic mass balance (Eq. 2), because they carry different isotopic signatures. This isotopic "disequilibrium" between photosynthetic and respiration fluxes arises from the rapidly decreasing (~ -5 ‰ yr^{-1}) background $\Delta^{14}CO_2$ (e.g., Lehman, 2013; Graven et al., 2020). Δ_{resp} is more positive than Δ_{photo} because Δ_{resp} is associated with biospheric CO_2 fixed by photosynthesis when the ambient atmospheric $\Delta^{14}CO_2$ (i.e. Δ_{bg}) was higher. Δ_{photo} is assumed equal to Δ_{bg} because the 'Δ' notation accounts for mass-dependent fractionation processes such as those occurring during photosynthesis. Turnbull et al. (2009) note that this assumption is valid in the limit that time and space between background and observation tends to zero. There is also a small impact on Δ_{obs} from pure ^{14}C emitted from certain nuclear reactors, which is added as the last term in Equation 2 (Graven and Gruber, 2011). Because this term is significantly smaller than all other terms in Equation (1), it is omitted there. Here N is the mass dependent Δ normalization factor, which is close to 1 (Basu et al., 2016). $^{14}C_{nuc}$ is the mole fraction of $\Delta^{14}CO_2$ resulting from the ^{14}C flux from reactors and R_{std} is the standard material $^{14}C/C$ ratio.

Combining Equations (1) and (2) results in:

$$CO_{2ff} = \frac{CO_{2obs}(\Delta_{obs}-\Delta_{bg})}{(\Delta_{ff}-\Delta_{bg})} - \frac{CO_{2resp}(\Delta_{resp}-\Delta_{bg})}{(\Delta_{ff}-\Delta_{bg})} - N^{14}C_{nuc}/R_{std}/(\Delta_{ff}-\Delta_{bg}). \tag{3}$$

The variables in Eq. (3) are either known or can be measured or calculated directly. Historically, CO_{2ff} has been approximated by only the first term on the right-hand side of Equation (3) (Levin et al., 2003). Disequilibrium and nuclear fluxes both add ^{14}C to the atmosphere. A correction (CO_{2corr}) is made to CO_{2ff} (Turnbull et al., 2009) to unmask these effects and reveal the full magnitude of the fossil fuel-CO_2 emissions signal, making it somewhat convenient to rewrite Equation (3) as:

$$CO_{2ff} = \frac{CO_{2obs}(\Delta_{obs}-\Delta_{bg})}{(\Delta_{ff}-\Delta_{bg})} - CO_{2corr}. \tag{4}$$

Flask ABL measurements for CO_{2obs} are defined as those samples collected at altitudes less than 1500 m ASL for all ACT flight campaigns. ABL samples typically contain the strongest regional flux signatures, and thus are likely to yield the largest $\Delta^{14}C$ signals. Conversely, we determine daily Δ_{bg} and CO_{2bg} values from measurements of $^{14}CO_2$ and CO_2 in flasks sampled at altitudes greater than 4000 m ASL for all flight campaigns to capture air that is within the well-mixed FT in all seasons. The FT data, while perhaps not always representative of the true, local-scale background signature (e.g. Turnbull et al., 2015), is expected to provide a reliable estimate of the regional- to continental-scale background (Baier et al., 2020). Here, Δ_{bg} in Eq. 2 is derived as the daily mean FT $\Delta^{14}CO_2$, typically between 4000 and 9000 m ASL. All flask FT measurements are filtered to remove samples with high CO (above three standard deviations from a smooth curve fit), which can indicate the potential

215 influence of local pollution on continental background values. Similarly, CO_{2bg} and other trace gas background mole fractions were derived as mean mole fractions of FT values for these species. For the ACT study, CO_{2corr} is derived for each flask sample by convolving estimated gridded monthly disequilibrium fluxes of $\Delta^{14}CO_2$ from the terrestrial biosphere and fluxes from nuclear reactors with surface influence functions for each flask sample location (i.e., for each flask "receptor", per below).

220 Surface influence functions (referred to as "footprints"), representing the sensitivity of air parcels at a particular receptor location to upwind surface fluxes (in units of ppm m^2 s μmol^{-1}), are derived by first using the Hybrid Single-Particle Lagrangian Integrated Trajectory (HYSPLIT) model (Draxler and Hess, 1997) running 500 randomly perturbed, 10-day back trajectories for all ABL flask receptors. Back trajectories are driven by 27-km horizontal resolution Weather Research and Forecasting (WRF) meteorological fields, nudged to the ERA-5 reanalysis meteorology within the ACT-America North American model
225 domain (Feng at al., 2021b, see Section 2.4). Individual footprints are calculated for all 500-particle trajectory ensemble members based on their residence time over a given gridded area (Lin et al, 2003) within the surface boundary, defined as a vertical column of air in each 1º x 1º grid cell between 125 m AGL and 50% of the WRF-calculated atmospheric boundary layer height (Fig. 1). Referring to Eqns. (1) and (2), though there exists a footprint signature on flask samples during fall 2017 and spring 2018, this influence is relatively small. Disequilibrium fluxes from the terrestrial biosphere are derived by
230 convolving impulse-response functions from the CASA biogeochemical model (Thompson and Randerson, 1999) with the atmospheric history of ^{14}C (Miller et al. 2012; LaFranchi et al., 2016, with updates in Zhou et al., 2020) while nuclear reactor fluxes are obtained from Graven and Gruber (2011), effectively assuming regional nuclear $^{14}CO_2$ has not changed significantly over time through 2019. These gridded fluxes (monthly, time-dependent in the case of disequilibrium flux) are converted to the two components of CO_{2corr} via convolution with footprints derived from HYSPLIT and are calculated individually for each
235 ABL flask sample pair for which CO_{2ff} is derived using Equation (4). We note that the calculated magnitude of CO_{2corr} attributable to nuclear reactor emissions in the Mid-Atlantic U.S. is 0.25 ± 0.44 ppm CO_2 and does not exhibit a seasonal pattern as it is assumed constant annually. Graven and Gruber (2011) have been used at the time that this publication was written, but updates to nuclear reactor fluxes have been published in Zazzeri et al. (2023). The magnitude of CO_{2corr} attributable to the terrestrial biosphere in the Mid-Atlantic U.S. is approximately 0.10 ± 0.04 ppm CO_{2ff} (1σ) during the winter deployment
240 and exhibits a seasonal cycle with a maximum during the summer of 0.70 ± 0.28 ppm CO_{2ff} (1σ), indicating similar seasonal behavior as that calculated by Miller et al. (2012) for the Mid-Atlantic U.S. In total, the average magnitude of CO_{2corr} (0.8 ± 0.6 ppm) calculated here to correct CO_{2ff} in this work is roughly comparable that first described in Turnbull et al. (2006).

2.4 Forward model CO_{2ff} using the PSUWRF model

A separate, Eulerian 27 km horizontal resolution implementation of WRF-Chem version 3.6.1 run (Feng et al., 2021a,b) was
245 implemented by the Pennsylvania State University (hereby called PSUWRF) with 50 vertical levels from the surface to 50 hPa, with 29 of these vertical levels in the lowermost 2 km. PSUWRF was developed and implemented during the ACT time

period (2016-2019) to simulate atmospheric transport of CO_2 component fluxes along all flight tracks for each seasonal campaign. Note that, while the Lagrangian HYSPLIT model mentioned above to calculate CO_{2corr} in Equation 4 for each flask measurement also used WRF for input meteorological fields, this was not identical to PSUWRF used for the Eulerian simulations. PSUWRF model runs were implemented prior to this manuscript development and could not be re-run, but both WRF versions used similar setups and thus we expect there to be no major inconsistencies between the use of these two different versions for calculating CO_{2ff} using flask or model output.

PSUWRF separately simulates the contributions of CO_2 boundary conditions, and biogenic, ocean, fossil fuel and biomass burning CO_2 fluxes to total CO_2 at any time and location in the model domain (Feng et al., 2019a,b). The microphysics, PBL and cumulus parameterization schemes used in this run are Thompson microphysics, the Mellor-Yamada-Nakanishi-Nino version 2 (MYNN2), and the Kain-Fritsch schemes, respectively (Feng et al., 2019a). As the ACT campaigns spanned multiple years, CO_2 oceanic, fossil fuel and biomass burning fluxes, and total CO_2 boundary conditions come from CarbonTracker version 2017 (CT2017) through 2017 and CT-NRTv2019-2 (Jacobson et al., 2020) afterwards. CT2017 and CT-NRTv2019-2 together are called 'CT' for simplicity. The CT fossil fuel tracer typically is derived from an average of the ODIAC and Miller emissions datasets. As both datasets have very similar global and national fossil fuel emissions totals, but include differences spatial and temporal emissions distributions, an average of the two is used in CT to optimize the mapping of these emissions (Jacobson et al., 2020). In PSUWRF, ODIAC and Miller datasets were run separately for initial model runs between 2016-2018 to experimentally investigate potential differences between the two; however, only small differences within ~2 ppm CO_{2ff} are seen between the two and are not expected to create inconsistencies in CO_{2ff} simulated by PSUWRF between 2016-2019. As such, ODIAC and Miller are averaged to create a single flux product and to simplify model runs as in CT for 2019. In PSUWRF, simulated fossil fuel CO_2 (CO_{2ffmod}) is calculated using the same approach as flask CO_{2ff}, where average FT values of this tracer are subtracted from ABL values. The PSUWRF model transport is nudged to ERA5 reanalysis data to improve the depiction of atmospheric transport relative to ACT in-flight meteorological observations (Gerken et al., 2021). PSUWRF model output was extracted to ACT research flight track locations at hourly resolution for comparison and evaluation relative to high-frequency, measurement-based CO_{2ff} described in Section 2.5.

2.5 Calculation of "pseudo" CO_{2ff}

As in previous studies (Levin and Karstens, 2007; Vogel et al., 2010; Turnbull et al., 2011a, Maier et al., 2024a), we employ in situ CO measurements for estimating CO_{2ff} (referred to as "pseudo-CO_{2ff}" and denoted as CO_{2ff}') at high temporal resolution. ACT in situ CO measurements were made by cavity ring-down spectroscopy at 0.4 Hz, drift-corrected during flight and calibrated once weekly using gas standards on the World Meteorological Organization (WMO) X2014A CO scale, just as NOAA flask-based measurements (Wei et al., 2020; DiGangi et al., 2021). After calibration, CO data were averaged to 0.2 Hz, the maximum frequency of CO_{2ff}'. We calculate CO_{2ff}' using Equation (5) by applying a median ratio of CO to CO_{2ff} (R_{CO})

calculated strictly from flask samples collected each day (typically from 5-12 flask samples), and apply this value to the in situ CO time series collected on that day's ACT research flight:

$$CO_{2ff}' = \frac{CO_{obs}' - \overline{CO'_{bg}}}{R_{CO}}.$$ (5)

Here, CO_{obs}' are 0.2 Hz ABL (below 1500 m ASL) in situ CO dry mole fraction observations and $\overline{CO'_{bg}}$ is the mean daily CO mole fraction observed in the FT (above 4000 m ASL) for each flight day. R_{CO} is calculated as median value of all flask measurements each day, i:

$$R_{CO} = \frac{[CO_{obs,flask} - \overline{CO_{bg,flask}}]_i}{CO_{2ff,flask\_i}}.$$ (6)

A median R_{CO} is used each day due to difficulty with respect to calculating seasonal regression slopes with low correlations (seasonal R^2 between 0.08-0.33) in the flask CO enhancement and CO_{2ff} data. In calculating daily median R_{CO}, it may be possible to capture some spatial variability of research flight observations rather than ignoring this variability and rely on average seasonal values. However, we acknowledge in Section 3.3.1 that this methodology, given low signal to noise ($\Delta^{14}CO_2$ precision) in the ACT CO_{2ff} data, could create anomalous variability in R_{CO} and is one of the largest sources of uncertainty in this CO_{2ff}' calculation (as first presented in detail in Maier et al., 2024b) and a limitation to this analysis. In situ FT measurements are filtered to remove high CO or local emissions influence. Similar to above, data with CO greater than three standard deviations from a smooth curve fit to background values are filtered. Each of these terms is derived exactly as the analysis of flask CO_{2ff} above. Due to the limited number of flasks sampled on each flight, R_{CO} is calculated as a daily median ratio of CO enhancements to CO_{2ff} from flask samples, and we assume that this ratio is representative of the entire flight region each day. In the analysis that follows, we assess the utility of this "pseudo-CO_{2ff}" method for determining fossil fuel CO_2 in evaluating modeled CO_{2ff} over larger regions where routine, high-density discrete flask sampling is not available. In this work, CO_{2ff}' is calculated only for flights when flask measurements were sampled and analyzed for $\Delta^{14}CO_2$ in order to reduce errors associated with assumptions in R_{CO} spatial and temporal variability.

2.6 CO_{2ff} uncertainty derivation

The total estimated uncertainty in CO_{2ff} is determined by a propagation of estimated uncertainties for individual budget terms through Equation (4). Flask-based CO_{2obs} and Δ_{obs} measurement uncertainties are 0.1 ppm and 1.8‰, respectively. Here Δ_{ff} is, by definition -1000‰, and carries no uncertainty. The uncertainty in Δ_{bg} is calculated through propagation of error in a) Δ_{obs} and b) the mean diurnal standard deviation of FT $\Delta^{14}CO_2$ observations (Δ_{bg}) for each ACT flight. The relative uncertainty in CO_{2corr} associated with biospheric disequilibrium and nuclear reactor fluxes is assumed to be 50% for each term. Daily

aggregated CO_{2ff} sample uncertainties are determined by using a 1,000-member Monte Carlo simulation that propagates these uncertainties through Equation (4) to provide an estimate of the flask-derived CO_{2ff} uncertainty per research flight. The average campaign-wide CO_{2ff} uncertainty (from the inner 68% confidence interval of the 1000-member CO_{2ff} normal distribution per research flight) is 1.22 ppm.

Similar to above, we calculate an average campaign uncertainty in CO_{2ff}' of 4.96 ppm (from the inner 68% confidence interval in CO_{2ff}' of a 1,000-member Monte Carlo approach for each flight day) using Equation (5). We estimate daily uncertainties by conservatively incorporating the CO dry mole fraction measurement precision on 0.2 Hz measurements (5 ppb), the uncertainty in daily background CO from CO_{obs} and the daily standard deviation in FT CO, and the uncertainty in R_{CO} from the width of a normally-distributed 68% confidence interval about average R_{CO} values.

The uncertainty in both CO_{2ff} and CO_{2ff}' is higher for ACT research flights due to the uncertainty caused by using a single CO or $\Delta^{14}CO_2$ background value for each flight, when in truth, different sectors of a research flight (e.g. the cold and warm sectors during frontal crossing flights) could experience different background conditions or could be influenced by deep convective mixing, violating the assumption that the continental background value is described by the FT value. Elevating the altitude threshold at which background values are defined (i.e. 4000 m ASL) can better isolate continental background air from lower tropospheric air that has been mixed with local emissions sources. However, using a higher threshold altitude to define background values can also lead to higher uncertainties in air that is considered as a background for local ABL measurements due to the fact that air at or above 4000 m ASL may have experienced longer-range transport.

3 Results and Discussion

3.1 Mid-Atlantic $\Delta^{14}CO_2$ background in general agreement with NOAA aircraft network

Figure 2a shows the vertical distribution of $\Delta^{14}CO_2$ measured for all seasonal campaigns between winter 2017 and summer 2019, highlighting this difference and indicating generally lower values and significantly greater variation relative to the FT throughout the bottommost troposphere due to surface emissions of ^{14}C-free fossil fuels.
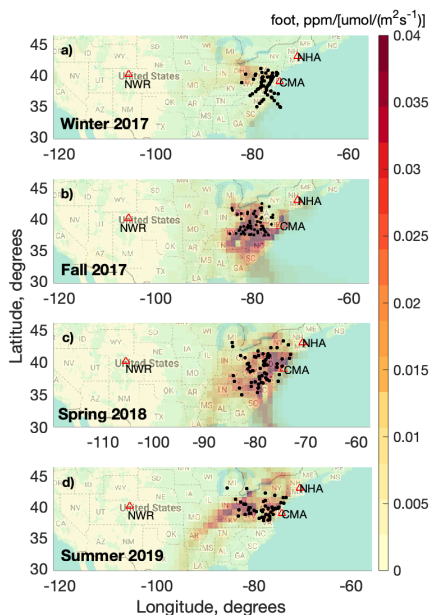
Figure 1. Surface influence for ABL $\Delta^{14}CO_2$ samples measured for ACT seasonal deployments in a) winter 2017, b) fall 2017, c) spring 2018, and d) summer 2019. ABL flask sample locations are denoted in black, with GGGRN Aircraft Program network sites indicated at Niwot Ridge, CO (NWR), Cape May, NJ (CMA), and Portsmouth, NH (NHA). Plot maps are produced using Google Maps API (©Google Maps).

Figure 2b shows the decrease in atmospheric $\Delta^{14}CO_2$ in the FT over time during ACT and within the broader NOAA Global Greenhouse Gas Reference Network (GGGRN) due to global-scale addition of fossil fuel CO_2 and justifies the use of ACT FT for a definition of background atmospheric conditions. As expected, values of Δ_{bg} throughout the upper FT are relatively homogenous during each campaign and are in rough agreement with other FT flask $\Delta^{14}CO_2$ measurements within the GGGRN (Sweeney et al., 2015; Miller et al., 2012) such as Cape May, NJ (CMA) and Portsmouth, NH (NHA). For fall and spring seasons, ACT FT $\Delta^{14}CO_2$ is slightly higher than that in the GGGRN sites, including the upwind, high-altitude (3000-4000 MASL) Niwot Ridge, CO (NWR) site. During ACT, FT samples are frequently obtained from higher altitudes than the GGGRN $\Delta^{14}CO_2$ paired flask samples with fixed collection altitudes, resulting in the potential for ACT FT air to originate from different latitudes or altitudes where influence from cosmogenically-produced $^{14}CO_2$ could explain deviations of ~ 2‰ above GGGRN $\Delta^{14}CO_2$ observations (Turnbull et al., 2009). Early in the ACT winter 2017 campaign, FT $\Delta^{14}CO_2$ is lower than the mean values in the GGGRN (Fig. 2b), and is accompanied by higher than average CO mole fractions. This result potentially indicates a small influence from local pollution sources that are depleted in FT $\Delta^{14}CO_2$. Nonetheless, these ACT FT data agree with (± 1σ standard deviation) GGGRN continental background FT values and are included in this analysis.
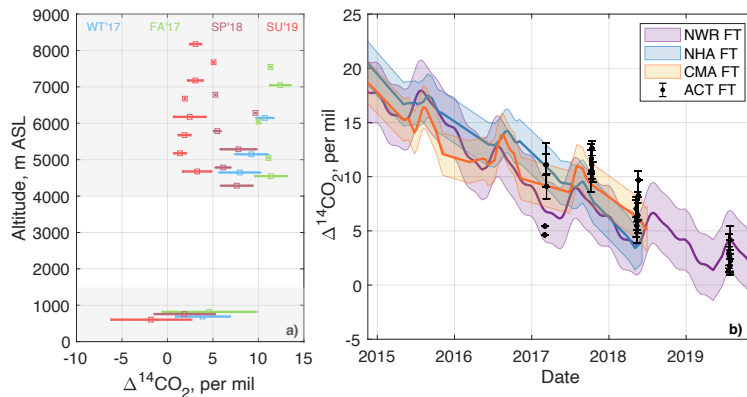
Figure 2. a): Vertical distribution of $\Delta^{14}CO_2$ during all ACT campaigns in the Mid-Atlantic U.S. ABL values shown are the average of all observations below 1500 m ASL (values are separated vertically for clarity) for each seasonal campaign while horizontal bars represent their 1σ standard deviation in time. FT values (altitudes greater than 4000 m ASL) shown are 500-m binned averages and their 1σ standard deviation in $\Delta^{14}CO_2$ for each 500 m altitude bin. Shaded regions represent ABL and FT definitions. b): Daily mean ACT FT $\Delta^{14}CO_2$ background measurements (± 1σ standard deviation shading) compared to NOAA GGGRN aircraft network $\Delta^{14}CO_2$ FT (~4000 m ASL) measurements. GGGRN data are seasonal (3-month averaged) aircraft FT $^{14}CO_2$ obtained offshore of Cape May, NJ (CMA) and offshore of Portsmouth, New Hampshire (NHA) and surface $\Delta^{14}CO_2$ for the high-altitude site, Niwot Ridge, CO (NWR) at ~3500 m ASL.

Figure 3a highlights the spatial extent of flask sampling during the ACT mission and density of flask sampling over the four seasonal campaigns with an average $\Delta^{14}CO_2$ ABL-FT difference of -5‰. Using Equation (4), CO_{2ff} is calculated for all flask samples, and general agreement between largely negative $\Delta^{14}CO_2$ ABL signals and higher CO_{2ff} signals are seen throughout

385 ACT (Fig. 3b). ACT observed CO_{2ff} ranges from -0.8 to 15.5 ppm, noting that negative CO_{2ff} values are not physically realistic but can occur due to the measurement uncertainty of $\Delta^{14}CO_2$, by using an inappropriate $\Delta^{14}CO_2$ background value, or by underestimating the CO_{2corr} term in Eq. 4. Compared to other surface and aircraft observations of CO_{2ff} throughout the U.S., the range of ACT CO_{2ff} is comparable to CO_{2ff} measured in other studies in the Mid-Atlantic U.S. (Miller et al., 2012: -3-13 ppm CO_{2ff}), downwind of Sacramento, CA (Turnbull et al., 2011a: 2.4-8.6 ppm CO_{2ff}) and in Colorado urban regions (Graven

390 et al., 2009: 0-20 ppm CO_{2ff}). Maximum values of CO_{2ff} measured during ACT were however much lower than those over the densely populated urban area of Los Angeles, CA (Miller et al., 2020: -1.3-48.4 ppm CO_{2ff}) due to its more rural sampling

focus. Few ACT flight legs were aimed at capturing local, urban-scale CO_{2ff} signals. As such, the analysis below requires averaging of these signals as a more robust way to qualitatively analyze the ACT flask CO_{2ff} data.

395
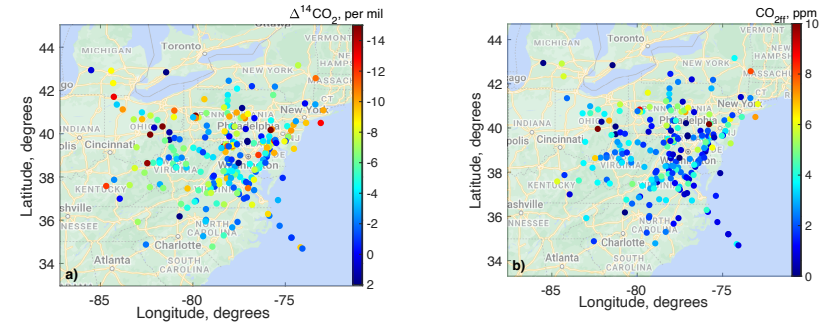
Figure 3: a) $\Delta^{14}CO_2$ ABL-FT differences for all seasons in the Mid-Atlantic U.S. Note that the color bar is reversed to indicate warmer colors for more negative $\Delta^{14}CO_2$. b) ABL CO_{2ff} calculated for the same flask samples shown in a) for all seasons in the Mid-Atlantic U.S. Plot maps are produced using Google Maps API (©Google Maps).

3.2 Partitioning of seasonal CO_{2tot} indicates biogenic-driven variability

For consistency throughout ACT seasonal campaigns, ABL values for all species in the subsequent analysis are reported as an ABL-FT difference. Figure 4 shows CO_{2ff}, alongside biogenic CO_2 (CO_{2bio}) calculated from Equation (1), displayed by month of the year for ACT deployments in winter (2017), spring (2018), summer (2019) and fall (2017) in the Mid-Atlantic United

400 States. Total (CO_{2tot}), fossil fuel and biogenic CO_2 are shown to indicate relative contributions to the observed CO_{2tot} variability (Eq. 1). CO_{2tot} observed in the ABL varies seasonally; while most often positive for flights conducted in late fall and winter, CO_2 depletion is seen during summer as expected due to net photosynthetic uptake by the terrestrial biosphere (Tans et al., 1990). Seasonal changes in ABL CO_{2tot} were driven by CO_{2bio}, which varied from -19.7 ppm during summer flights to 16.2 ppm in late fall (Fig. 4). In early fall, negative CO_{2bio} was observed (Fig. 4) from strong surface influence and net uptake in

405 southwestern Virginia (Fig. 1). For the remainder of the fall campaign, flights indicated generally positive CO_{2bio} with net respiration and weaker surface influence. CO_{2ff} has a lower contribution to CO_{2tot} variability during ACT in the Mid-Atlantic region from one campaign to the next, with a positive contribution of 3.3 ± 2.0 ppm. Given the small number of flights shown over three years, it should be noted that the seasonality in CO_{2ff} may not represent true climatological CO_{2ff} variability and should not be interpreted in terms of uniform fossil fuel emissions because there is likely seasonal variation in ABL depth,

410 which can counteract seasonally-varying emissions.
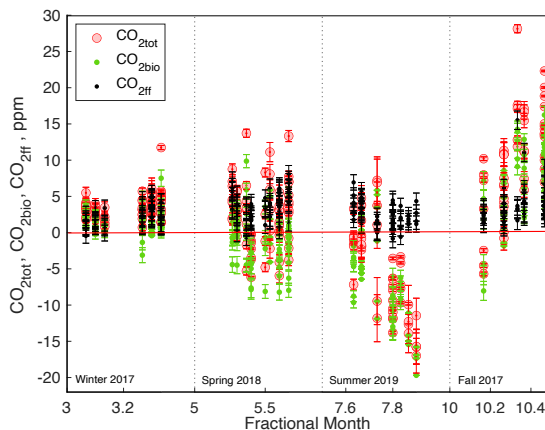
Figure 4. Calculated total CO₂ (CO₂tot), partitioned into biogenic CO₂ (CO₂bio) and fossil fuel CO₂ (CO₂ff) components using Eq. (4) in winter 2017; spring 2018; summer 2019; and fall 2017. As seasonal campaigns were not conducted consecutively within a single year, we examine variability according to a "climatological" year. Note that the x-axis is intentionally non-linear to show intra-day variability. One sigma error bars are shown for CO₂tot, CO₂bio, and CO₂ff.

The flask sampling region for this study encompasses rural to suburban regions, reducing signal to noise in $\Delta^{14}CO_2$ and complicating the interpretation of CO_{2tot} observed due to a wide mixture of surface sources (and sinks). As CO_{2tot} is largely controlled by CO_{2bio}, we correlate (using Pearson's R^2 values) and regress CO_{2tot} with CO_{2ff} and with CO_{2bio} (see Table S1 of supplementary material). Regressions between CO_{2bio} and CO_{2tot} result in slopes between 0.86 and 0.92 for all seasons. Strong correlations between CO_{2bio} and CO_{2tot} exist from spring through fall with R^2 values between 0.73 and 0.92. Somewhat strong relationships between CO_{2tot} and CO_{2bio} were found during the March winter 2017 campaign with a regression slope close to 1 but relatively weak correlation ($R^2 \sim 0.3$), which could partially be explained by small CO_{2ff} signals, but also indicate that observed CO_2 had a non-negligible influence from biogenic CO_2 exchange as was also found in previous studies (Potosnak et al., 1999; Turnbull et al., 2006; Miller et al., 2012; Baier et al., 2020). Correlations between CO_{2tot} and CO_{2ff} are weak, with associated regression slopes highest during winter and smaller slopes observed for the spring, summer, and fall deployments when ecosystem CO_2 fluxes are higher.

Deleted: indicating

The fraction of negative CO_{2tot} during biogenically active months in spring (May), summer (July), and fall (October) are 28%, 62%, and 4%, respectively (Table S1). However, when examining the fraction of negative CO_{2bio} (indicating net CO_2 uptake), these percentages are much larger at 57%, 82%, and 8%, respectively. The difference between negative CO_{2tot} and negative CO_{2bio} fractions of 20-30% during months when the ecosystems are more active highlights the importance of using $\Delta^{14}CO_2$ to

430 enable partitioning of CO_{2tot} into fossil fuel and biogenic components; this would not be possible when considering CO_{2tot} alone, as a portion of this flux component would be masked by fossil fuel emissions.
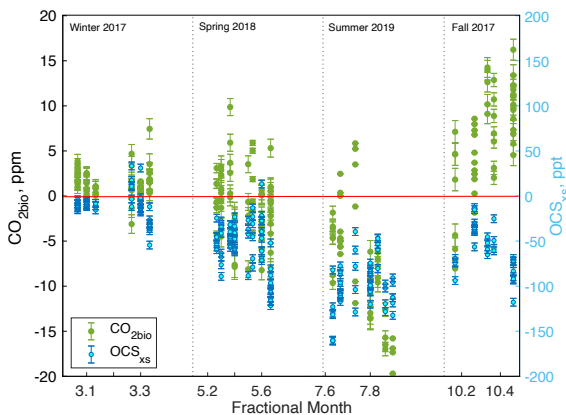
Figure 5. ABL biogenic CO_2 (CO_{2bio}) and OCS ABL-FT difference (OCS_{xs}) in winter 2017; spring 2018; summer 2019; and fall 2017. As seasonal campaigns were not conducted consecutively within a single year, we examine variability according to a "climatological" year. Note that the x-axis is intentionally non-linear to show intra-day variability. One sigma error bars are shown for CO_{2bio} and OCS_{xs}.

We also examine carbonyl sulfide ABL-FT differences (OCS_{xs}) alongside CO_{2bio} as an additional tracer for biogenic processing as OCS is taken up by plants similarly to CO_2 but not respired (Montzka et al., 2007; Campbell et al., 2008, Fig. 5). In Figure

435 5, we observe a strong positive correlation with CO_{2bio} and OCS_{xs} when combining all seasonal ACT data except fall where CO_{2bio} is either negative or weakly positive (see Fig. S1a of supplementary material), consistent with photosynthesis explaining negative CO_{2bio} values. A modest positive correlation (R = 0.54) is seen when also including fall ACT data. Including or excluding the winter data, given the insignificant slope between OCS_{xs} and CO_{2bio} (Table S1), does not affect this correlation.

440 For fall 2017, the overall correlation between CO_{2bio} and OCS_{xs} is low and not significant (Table S1). However, statistically significant correlations are seen between negative CO_{2bio} and OCS_{xs} in early fall due to continued uptake of CO_2 by the terrestrial biosphere (Fig. 5). A moderate negative correlation is observed between OCS_{xs} and CO_{2bio} in late fall after net respiration is seen to occur (Fig. 5, Fig. S1b). During this time, CO_{2bio} of up to ~16 ppm occurs alongside relatively significant
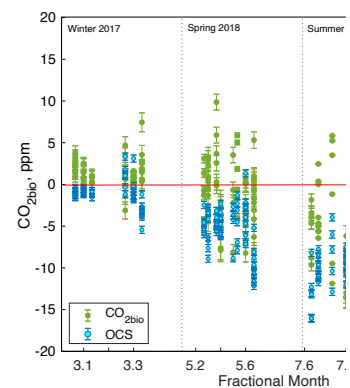
OCS$_{xs}$ of almost -120 ppt. The net negative correlation during fall between CO$_{2bio}$ and OCS$_{xs}$ indicates that, while CO$_2$ uptake could still be occurring, the magnitude of this process is not large enough to offset respiration. Similar to ACT, clear differences in the amplitude and phases of OCS and CO$_2$ cycles were first described in Montzka et al. (2007) and in other, previous studies (Kuai et al., 2022, Ma et al., 2023). Furthermore, many OCS studies have found several instances where ecosystem OCS uptake is decoupled from GPP, including nighttime processes (Commane et al., 2015; Kooijmans et al., 2017; Hu et al., 2021), uptake from soil (Whelan et al., 2022) and/or from senescing or decaying fall vegetation (Sun et al., 2016; Rastogi et al., 2018). Further studies could utilize collocated measurements such as OCS and radiocarbon-based CO$_{2bio}$ to evaluate a) the relationship between OCS and CO$_2$ cycles during the transition from net photosynthesis to net respiration and b) regional model GPP and respiration fluxes. Further, we note that correlations between negative CO$_{2tot}$ and OCS$_{xs}$ weaken in the early fall due to proportionally high fossil fuel emissions, providing insufficient information about GPP. Parazoo et al. (2021) found that models underestimate observed CO$_{2tot}$ during ACT, and have decreased fidelity in reproducing GPP inferred from observations throughout the U.S. Since stronger relationships emerge between OCS$_{xs}$ and CO$_{2bio}$ than OCS$_{xs}$ and CO$_{2tot}$, again, using OCS and radiocarbon-based CO$_{2bio}$ could further inform and constrain these model processes.

3.3 Example Case: "Pseudo-CO$_{2ff}$" as a product for evaluating model error

We use CO$_{2ff}$ as a model "transport tracer", to examine model errors as CO$_{2ff}$ fluxes are assumed to be relatively well-known (Turnbull et al., 2009). Well-known emissions and well-measured mole fractions directly tracing those emissions allow us to evaluate the atmospheric tracer transport that connects the two. Here, we compare a "pseudo-CO$_{2ff}$" or high-frequency CO$_{2ff}$' (Equation 5) to CO$_{2ffmod}$ simulated using the PSUWRF forward model, based on Miller fossil fuel emissions (Jacobson et al., 2020). This CO$_{2ff}$' product being high-frequency can also capture more diurnal variability in fossil fuel CO$_2$, and therefore evaluate modeled fossil fuel CO$_2$ more thoroughly, than measurements made using discrete flask samples.

3.3.1 Variability and uncertainty of R$_{CO}$ and CO$_{2ff}$

Our CO$_{2ff}$' estimation relies on the assumption that the emission ratio of CO to CO$_{2ff}$ (R$_{CO}$) is constant for a given flight day. As mentioned above, a median R$_{CO}$ value for each day is used as opposed to a more general, regression slope between flask CO ABL-FT differences and CO$_{2ff}$ because of low correlations between the two variables seasonally. We note that the numerator of R$_{CO}$ represents the enhancement in all CO sources (fossil, but also potentially biomass burning and oxidation of volatile organic compounds (VOCs)) as well as a very small amount of CO oxidative loss. Because all of these sources are "calibrated" relative to CO$_{2ff}$ (the denominator), it is not necessary to explicitly define non-fossil components of this ratio.
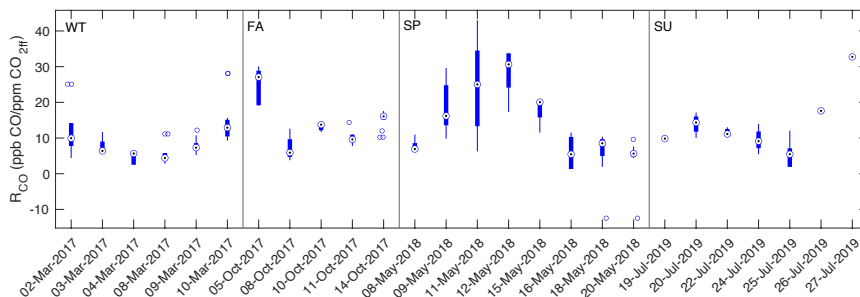
Figure 6. Daily R$_{CO}$ calculated from discrete flask samples during winter (WT, 2017), fall (FA, 2017), spring (SP, 2018), and summer (SU, 2019). Note that, unlike Figures 4 and 5, flight data is shown in chronological order. Median R$_{CO}$ for each research flight is shown as a bullet point, with the interquartile (IQ) range shown as the thick bar line. Outliers greater than 1.5 times the IQ range are shown as separate open circles, and maximum extreme values as "whiskers" that do not qualify as outliers (thin lines) extending from the IQ ranges. Flask data shown are combined for B-200 and C-130 aircraft.

Figure 6 indicates that the median R$_{CO}$ calculated for all ACT missions (10.03 ± 8.15 ΔCO per ppm CO$_{2ff}$; 68% CI) is slightly higher than in urban studies (Turnbull et al., 2011a; Miller et al., 2012; Turnbull et al., 2014). Day-to-day or even diurnal R$_{CO}$ is also largely variable, which could be a result of variability in CO$_{2ff}$, or in measured background levels (which are represented by a single daily value). Spatial differences in VOC oxidation could play a minor role in influencing the variability of R$_{CO}$. CO additions from VOCs throughout the ACT Mid-Atlantic region will render R$_{CO}$ higher. However, despite the expectation that greater oxidation of VOCs will produce more CO during the summer (Vimont et al., 2017), we see the highest average R$_{CO}$ values during spring. R$_{CO}$ variability in both the fall and spring campaigns suggest that there could be other influential mechanisms occurring, yet DiGangi et al. (2021) found that biomass burning influence on air sampled during ACT were negligible in the Mid-Atlantic region, ruling out the possibility that biomass burning events contribute to the high variability of R$_{CO}$ calculated here. In general, it is more likely that low CO$_{2ff}$ signals with high relative uncertainties are creating abnormally high R$_{CO}$ values using this median method in this work, which has also been found and discussed in great detail in Maier et al., (2024b).

As mentioned above, we calculate CO$_{2ff}$' only for days when flask measurements were analyzed for Δ^{14}CO$_2$. When comparing CO$_{2ff}$' with flask-based CO$_{2ff}$, the mean bias is 0.7±2.1 ppm (1σ) (Fig. 7). The relatively large standard deviation in Fig. 7 indicates that flask samples collected within a single research flight were not always representative of the entire domain surveyed on that day by continuous analyzers. Point sources of CO$_2$ from power plants that do not emit CO captured by

continuous measurements could potentially skew this comparison alongside other non-fossil fuel CO sources, but the small bias between the two suggests that CO_{2ff}' is generally in good agreement with flask CO_{2ff}.
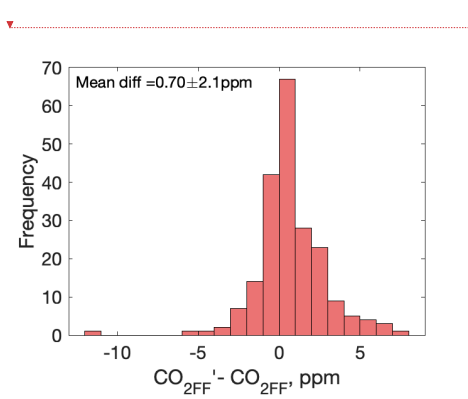
Figure 7. Histogram of in situ (CO_{2ff}') minus flask-derived (CO_{2ff}) fossil fuel CO_2 for total-campaign corresponding measurement times (winter 2017 through summer 2019) in the Mid-Atlantic region. Here, CO_{2ff}' is calculated for corresponding flask sample times. By definition of CO_{2ff} and CO_{2ff}' above, this comparison indicates ABL sample comparisons only.
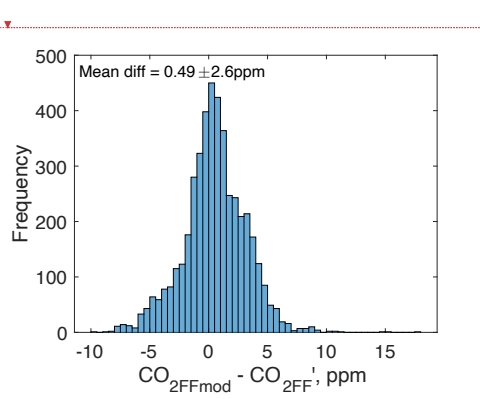
Figure 8. Histogram of PSUWRF $CO_{2ffmod} - CO_{2ff}'$ for all flask $\Delta^{14}CO_2$ sample days between winter 2017 and summer 2019 in the Mid-Atlantic region.

530 **3.3.2 Comparison of CO_{2ff}' and CO_{2ffmod}**

Figure 8 shows the average difference between CO_{2ffmod} computed along ACT flight tracks and ABL CO_{2ff}'. Several research flight days indicate rough agreement between CO_{2ffmod} and CO_{2ff}' within a mean of ~0.49±2.6 ppm (1σ), but higher differences outside of average CO_{2ff}' uncertainty bounds are seen in Fig. 8 along with a slight skewness. The mapped extent of this positive bias in CO_{2ffmod} is visualized in Figure 9 for fall 2017, spring 2018 and summer 2019 campaigns, while the winter

535 2017 campaign model bias in CO_{2ffmod} is slightly negative.
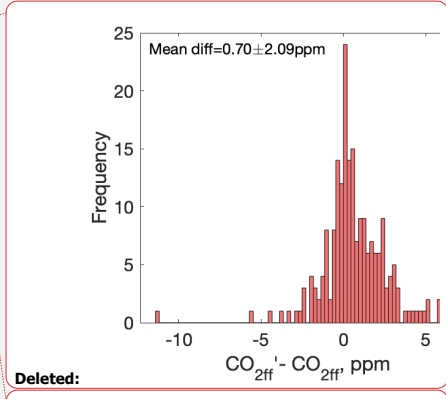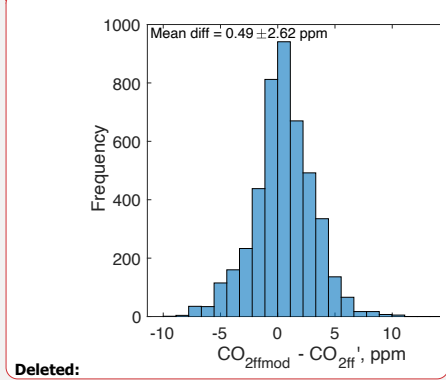
While there are logistical advantages to using this "pseudo-CO_{2ff}" method from a $\Delta^{14}CO_2$ measurement capacity standpoint, this product has a higher uncertainty (4.96 ppm) associated with large intra-day background variability and assumptions in the value of R_{CO}. For this reason, we caution the overgeneralization of the use of CO_{2ff} as a transport tracer with this dataset and have chosen July 24, 2019 as an example of where positively biased CO_{2ffmod} can be evaluated using CO_{2ff}'. Here, a series of 545 B-200 flights was conducted downwind of three major eastern U.S. cities (New York City, NY; Philadelphia, PA; and Washington, DC). ABL flask sampling on each flight leg informed the derivation of CO_{2ff}', and both estimates are in rough agreement as seen in Fig. 10. This individual flight day had higher fossil fuel CO_2 signals and lower variability in background CO measurements, with a lower CO_{2ff}' uncertainty of ~2 ppm relative to the campaign-wide average.

Deleted:
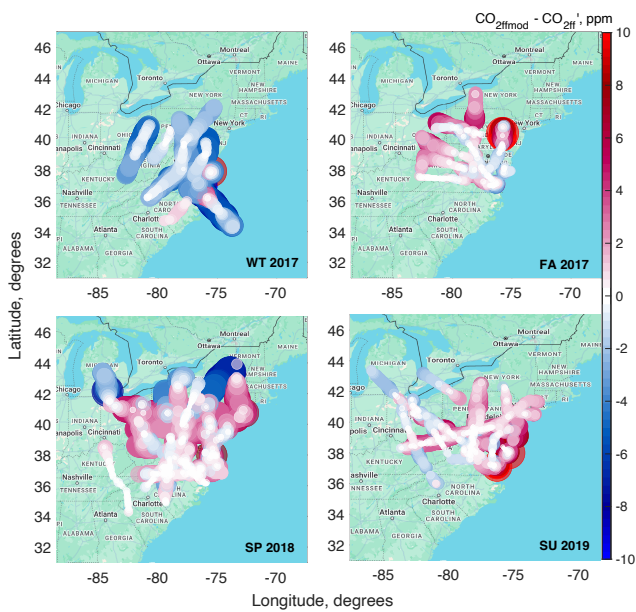
Figure 9. Mapped modeled versus CO_{2ff}' for flask $\Delta^{14}CO_2$ sample flight days for a) winter (WT) 2017, b) fall (FA) 2017, c) spring (SP) 2018 and d) summer (SU) 2019 campaigns. Points are sized by the model-data differences. Plot maps are produced using Google Maps API (©Google Maps).
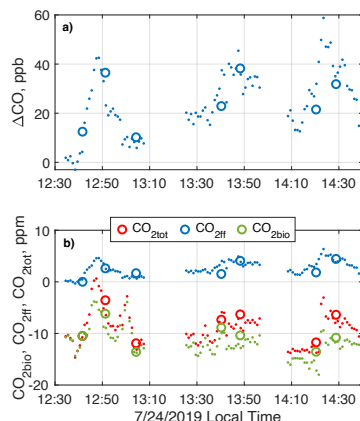
Figure 10. In situ (points) and flask (circles) observations for the B-200 aircraft on July 24, 2019. (a) CO ABL-FT differences (ΔCO) calculated from flasks and in situ continuous measurements. ΔCO from flasks is used to calculate R_{CO} and thus CO_{2ff}' using Eq. 5 using in situ measurements. The average difference in ΔCO (in situ – flask) is 0.6±8.7 ppb. (b) CO_{2bio}, CO_{2ff}', and CO_{2tot} calculated from both in situ high-frequency data (points) and from flask measurements (circles) on July 24, 2019 showing good agreement. Average differences in CO_{2bio}, CO_{2ff}', and CO_{2tot} (in situ – flask) are -1.6 ± 1.2 ppm, 1.2 ± 1.3 ppm and 0.4 ± 1.2ppm, respectively.
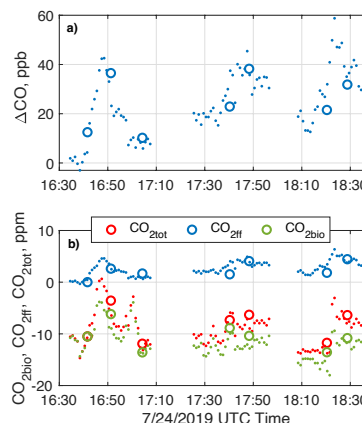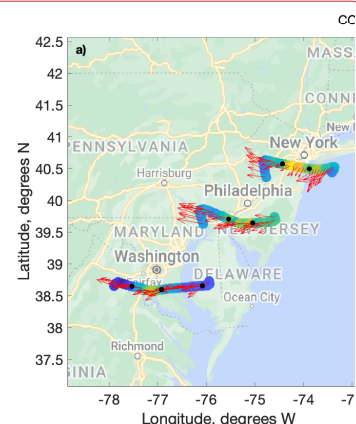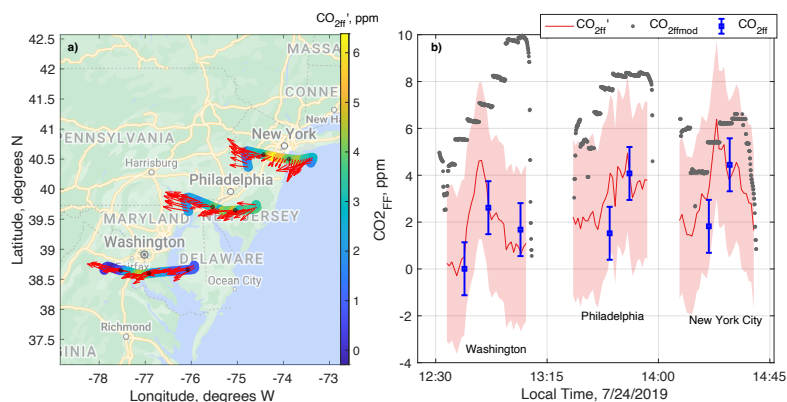
Figure 11. a) Pseudo-CO_{2ff} (CO_{2ff}') calculated along the ACT B-200 ABL flight track on July 24, 2019 (plot produced using Google Maps API, ©Google Maps). Flight tracks are colored by CO_{2ff}' which proceed northerly from Washington, DC to New York City, NY. Black points indicate flask sample locations. Red arrows indicate the wind direction as calculated from aircraft flight data. b) Fossil fuel CO_2 calculated from in situ measurements (CO_{2ff}'), from flask $\Delta^{14}CO_2$ (CO_{2ff}) and from PSUWRF using CT fossil fuel emissions (CO_{2ffmod}). Discretization in CO_{2ffmod} is due to the native 27-km resolution of PSUWRF. Error shading on

CO_{2FF}' is the derived 1σ uncertainty on the CO_{2ff}' calculation for July 24, 2019 and error bars on flask CO_{2ff} reflect a 1σ uncertainty.

Figure 11 shows calculated CO_{2ff}' along three ABL flight legs with large positive fossil fuel CO_2 downwind of these urban
555 areas. Comparing modeled (CO_{2ffmod}), calculated (CO_{2ff}'), and flask-derived (CO_{2ff}) CO_{2ff}, we find that CO_{2ff}' plumes observed downwind of cities do not always align with CO_{2ffmod} throughout the research flight. Significant differences are observed between CO_{2ffmod} and CO_{2ff}' magnitudes, particularly during the Washington, D.C. flight leg of up to 60% beyond uncertainty bounds, with the urban emissions plume misaligned (Fig. 11). CO_{2ffmod} is consistently higher than CO_{2ff}' in the Philadelphia flight leg as well, with general agreement in the plume variability. Finally, we note that the PSUWRF model simulates CO_{2ff}
560 in the New York City flight leg relatively well with respect to flask CO_{2ff}.

Current uncertainties of CO_2 fossil fuel fluxes, based on differences among various emissions products, are less than or equal to 20% at the regional scale (Gurney et al., 2020), and this is corroborated in the PSUWRF model, where Feng et al., (2019a) note that the uncertainty in fossil fuel fluxes on a daily average time scale is approximately 20%. This uncertainty may increase
565 at the hourly timescale and certainly within smaller, urban-scale domains (Gately and Hutyra, 2017). We investigate several reasons for the 60% overestimation in simulated CO_{2ff} beyond the larger calculated CO_{2ff}' uncertainty bounds and the misalignment of the Washington, D.C. CO_{2ffmod} "plume" relative to CO_{2ff}' could occur. First, this discrepancy cannot be explained by model deviations in key meteorological variables such as wind speed, wind direction or atmospheric boundary layer depth relative to observations. The PSUWRF modeled wind speeds and directions compare well to in situ wind speed
570 and directions along the B-200 flight track to within 1 m s^{-1} and 10 degrees, respectively. ABL depths derived from B-200 potential temperature soundings flown at the endpoints of each urban transect in Fig. 11 also compare well with ABL depth estimated from PSUWRF potential temperature to within 300 m on average. Second, emissions uncertainties within PSUWRF could result in observed differences between CO_{2ff}' and CO_{2ffmod} of this magnitude. One hypothesis is that, if multiple fossil fuel emissions datasets are run independently in PSUWRF and the ensemble of these simulations is narrow, then more
575 confidence can be gained in that the differences in Fig. 11 are not due to errors in fluxes, but rather in model transport. PSUWRF simulations between 2017-2018 indicate that independently-run fossil fuel emissions fields with differing spatial and temporal resolution (i.e. ODIAC and Miller fields) result in small CO_{2ffmod} differences that are within 1.5-2 ppm on average. While these fossil fuel emissions products were not run separately in the PSUWRF model beyond 2018, a 2 ppm CO_{2ffmod} variability is substantially smaller than that shown in Fig. 11 downwind of Washington and Philadelphia (3-6 ppm
580 CO_{2ff}). It is possible that the model vertical transport parameterizations are erroneous earlier in the day, which could produce errors later in the day in CO_{2ff} accumulation and venting relative to that observed downwind of Washington, D.C., and even Philadelphia, PA. Therefore, while our current results suggest that model transport, rather than fluxes are erroneous on this particular flight, the results from this case study are important to document for future model-observation comparisons. More intensive work beyond the scope of this work would be needed to verify our hypothesis, which could involve model runs with

a number of both transport and flux variants to discern model variability with different, realistic ensemble members. Within this type of study, observed and modeled values for additional urban campaign data should also be compared.

615

While this example does not represent the average CO_{2ffmod} bias with respect to CO_{2ff}' during ACT, it illustrates the utility of CO_{2ff} as a model transport tracer. In the above example, the high-frequency CO_{2ff}' product is able to easily highlight potential modeled errors in the representation of diurnal CO_{2ff} plume variability. As discussed in Miller et al. (2020), deriving CO_{2ff}' in this way, using information gleaned from a small subset of $\Delta^{14}CO_2$ flask sample measurements, can provide a means for

620 determining the fossil fuel and biogenic components of CO_{2tot} for regional or city-scale studies. Despite higher average uncertainties than flask-based methods, comparisons to models might allow for examination and improvements upon gross model errors for more accurate CO_2 mole fraction estimation and process-based studies. As mentioned above, differentiating between regional model transport and flux errors might be improved upon in the future by using an ensemble of both transport and flux variants. As ACT $\Delta^{14}CO_2$ flask sampling was generally aimed at capturing broad-scale biogenic CO_2 features across

625 the eastern U.S., more targeted flask sampling in urban areas with larger CO_{2ff} signals could reduce R_{CO} and CO_{2ff}' uncertainties, which would allow for more robust $\Delta^{14}CO_2$-based model verification using comparatively fewer flask samples. At more rural sites, a greater number of flask samples may be needed to robustly calculate CO_{2ff}' (Maier et al., 2024b).

4 Conclusions

The ACT-America mission, while focused on the improvement of the accuracy of regional carbon flux estimates, also provided

630 the opportunity for a dense, seasonally-diverse dataset of atmospheric $\Delta^{14}CO_2$ measurements from flasks sampled throughout the Mid-Atlantic U.S. and the capability to disaggregate total CO_2 into biogenic and fossil fuel components, which is critical for regional CO_2 source attribution. Seasonal campaigns occurring between 2017 and 2019 indicated that biogenic CO_2 exchange in the Mid-Atlantic was the primary driver of CO_2 boundary layer variability in this region as expected, while CO_{2ff} remained relatively constant during the ACT mission. Consistent OCS uptake in all seasons was observed that correlated well

635 with negative CO_{2bio}, confirming CO_2 uptake by photosynthesis throughout the ACT campaigns, though instances were seen where OCS uptake was clearly decoupled from gross primary productivity during the fall. With the broad nature of flask sampling during ACT, the signal to noise (measurement precision) ratio in $\Delta^{14}CO_2$ data was low and campaigns investigating strictly urban CO_2 signals can better highlight the utility that routine observations of $\Delta^{14}CO_2$ can provide, including critical information for stakeholders in assessing carbon reduction strategies on regional to sub-regional scales. Several studies have

640 shown the value of incorporating $\Delta^{14}CO_2$ alongside CO_2 measurements as an improved model constraint on regional CO_2 fluxes and future work will require a continued effort to ensure routine $\Delta^{14}CO_2$ measurements throughout the NOAA GGGRN and other networks. Here, we have used flask $\Delta^{14}CO_2$ samples, taken alongside continuous in situ CO measurements, to provide a high-frequency "pseudo-CO_{2ff}" product (CO_{2ff}') using the relationship between in situ CO ABL-FT differences and flask-

derived CO_{2ff}. This product was used to evaluate modeled CO_{2ff} at a higher temporal resolution than discrete flasks can provide, and to illuminate potential errors in model transport at the regional scale. Although the ACT dataset and analysis therein is limited by higher CO_{2ff}' uncertainties, and to days where $\Delta^{14}CO_2$ signals are higher, this work highlights the value of such a product in future campaigns and measurement networks as a model evaluation tool.

Data Availability

Observational in situ and flask data from the NASA ACT-America mission used for the analysis in this study are publicly archived at the Oak Ridge National Laboratory repository at https://doi.org/10.3334/ORNLDAAC/1593 (Davis et al., 2018) in addition to PSUWRF output for the ACT-America campaign at https://doi.org/10.3334/ORNLDAAC/1884 (Feng et al., 2021). Individual flask data with $^{14}CO_2$ measurements from ACT-America can be found at (https://doi.org/10.3334/ORNLDAAC/1575). All data are synced to meteorological and location data onboard each aircraft and available for downloading and merging (https://doi.org/10.3334/ORNLDAAC/1574). GGGRN $\Delta^{14}CO_2$ and CO flask data used to supplement this study from NWR, NHA, and CMA are available at https://doi.org/10.15138/87ny-6277. The NOAA HYSPLIT model is publicly available via https://www.ready.noaa.gov/HYSPLIT.php for registered and unregistered versions.

Author Contributions

BCB led the investigation and curated the data alongside JPD, YC, SL and CW. CS, KD, JM, JPD and SL assisted with acquiring funding for this work. BB, JM, and SL conceptualized the analysis and contributed to writing the original draft of this manuscript. SF and TL developed and contributed model analysis and output. All authors contributed to reviewing and editing the manuscript.

Competing Interests

The authors declare that they have no conflict of interest.

Acknowledgements

They acknowledge the collaboration between NOAA Global Monitoring Laboratory (GML) and its cooperative partners, including its collaboration with the Cooperative Institute for Research in Environmental Sciences (CIRES) and facilities available to the Institute for Arctic and Alpine Research (INSTAAR). The authors thank Jocelyn Turnbull and Stephen Montzka for helpful discussions of data analysis methods and to Zachary Barkley for conducting PSUWRF model-observation comparisons of meteorological variables. We also acknowledge the critical work of NOAA/GML personnel Patricia Lang, Andrew Crotwell, Monica Madronich, Eric Moglia, Benjamin R. Miller, Duane Kitzis and Molly Crotwell with the measurement of flask samples and calibration of measurements, and NOAA collaborative partners throughout the GGGRN with the collection of aircraft flask samples at CMA, NHA and NWR. We acknowledge that this work would not have been

made possible without significant help from the ACT-America science team, pilots, and NASA management support. Partial funding for this work was provided to the University of Colorado/CIRES from NASA grant NNX15AJ06G and the NOAA

710   Cooperative Agreement with CIRES, NA17OAR4320101 and by NASA's Earth Science Division grant NNX15AG76G to Penn State. S. Feng at PNNL is supported by the NASA Carbon Monitoring Program (Grant number: 80HQTR21T0069). The Pacific Northwest National Laboratory is operated by Battelle Memorial Institute under contract DE-A05-76RL0 1830.

References

Andres, R. J., Boden, T. A., Breon, F.-M., Ciais, P., Davis, S., Erickson, D., Gregg, J. S., Jacobson, A., Marland, G., Miller,
715   J., Oda, T., Oliver, J. G. J., Raupach, M. R., Rayner, P., and Treanton, K.: A synthesis of carbon dioxide emissions from fossil-fuel combustion, 2012.

Baier, B. C., Sweeney, C., Choi, Y., Davis, K. J., DiGangi, J. P., Feng, S., Fried, A., Halliday, H., Higgs, J., Lauvaux, T., Miller, B. R., Montzka, S. A., Newberger, T., Nowak, J. B., Patra, P., Richter, D., Walega, J., and Weibring, P.: Multispecies
720   Assessment of Factors Influencing Regional CO2 and CH4 Enhancements During the Winter 2017 ACT-America Campaign, Journal of Geophysical Research: Atmospheres, 125, e2019JD031339, https://doi.org/10.1029/2019JD031339, 2020.

Ballantyne, A. P., Alden, C. B., Miller, J. B., Tans, P. P., and White, J. W. C.: Increase in observed net carbon dioxide
725   uptake by land and oceans during the past 50 years, Nature, 488, 70–72, https://doi.org/10.1038/nature11299, 2012.

Baker, D. F., Law, R. M., Gurney, K. R., Rayner, P., Peylin, P., Denning, A. S., Bousquet, P., Bruhwiler, L., Chen, Y.-H., Ciais, P., Fung, I. Y., Heimann, M., John, J., Maki, T., Maksyutov, S., Masarie, K., Prather, M., Pak, B., Taguchi, S., and Zhu, Z.: TransCom 3 inversion intercomparison: Impact of transport model errors on the interannual variability of regional
730   CO2 fluxes, 1988–2003, Global Biogeochem. Cycles, 20, GB1002, https://doi.org/10.1029/2004GB002439, 2006.

Basu, S., Miller, J. B., and Lehman, S.: Separation of biospheric and fossil fuel fluxes of CO 2 by atmospheric inversion of CO 2 and 14 CO 2 measurements: Observation System Simulations, Atmospheric Chemistry and Physics; Katlenburg-Lindau, 16, 5665–5683, http://dx.doi.org/10.5194/acp-16-5665-2016, 2016.
735

Basu, S., Lehman, S. J., Miller, J. B., Andrews, A. E., Sweeney, C., Gurney, K. R., Xu, X., Southon, J., and Tans, P. P.: Estimating US fossil fuel CO2 emissions from measurements of 14C in atmospheric CO2, Proceedings of the National Academy of Sciences, 117, 13300–13307, https://doi.org/10.1073/pnas.1919032117, 2020.

740   Brophy, K., Graven, H., Manning, A. J., White, E., Arnold, T., Fischer, M. L., Jeong, S., Cui, X., and Rigby, M.: Characterizing uncertainties in atmospheric inversions of fossil fuel CO_2 emissions in California, Atmospheric Chemistry and Physics, 19, 2991–3006, https://doi.org/10.5194/acp-19-2991-2019, 2019.

745   Campbell, J. E., Carmichael, G. R., Chai, T., Mena-Carrasco, M., Tang, Y., Blake, D. R., Blake, N. J., Vay, S. A., Collatz, G. J., Baker, I., Berry, J. A., Montzka, S. A., Sweeney, C., Schnoor, J. L., and Stanier, C. O.: Photosynthetic Control of Atmospheric Carbonyl Sulfide During the Growing Season, Science, 322, 1085–1088, https://doi.org/10.1126/science.1164015, 2008.

Ciais, P., Rayner, P., Chevallier, F., Bousquet, P., Logan, M., Peylin, P., and Ramonet, M.: Atmospheric inversions for
estimating CO2 fluxes: methods and perspectives, Climatic Change, 103, 69–92, https://doi.org/10.1007/s10584-010-9909-3,
2010.

Commane, R., Meredith, L. K., Baker, I. T., Berry, J. A., Munger, J. W., Montzka, S. A., Templer, P. H., Juice, S. M.,
Zahniser, M. S., and Wofsy, S. C.: Seasonal fluxes of carbonyl sulfide in a midlatitude forest, Proceedings of the National
Academy of Sciences, 112, 14162–14167, https://doi.org/10.1073/pnas.1504131112, 2015.

Davis, K. J., Browell, E. V., Feng, S., Lauvaux, T., Obland, M. D., Pal, S., Baier, B. C., Baker, D. F., Baker, I. T., Barkley,
Z. R., Bowman, K. W., Cui, Y. Y., Denning, A. S., DiGangi, J. P., Dobler, J. T., Fried, A., Gerken, T., Keller, K., Lin, B.,
Nehrir, A. R., Normile, C. P., O'Dell, C. W., Ott, L. E., Roiger, A., Schuh, A. E., Sweeney, C., Wei, Y., Weir, B., Xue, M.,
and Williams, C. A.: The Atmospheric Carbon and Transport (ACT)-America Mission, Bulletin of the American
Meteorological Society, 102, E1714–E1734, https://doi.org/10.1175/BAMS-D-20-0300.1, 2021.

Davis, K. J., Obland, M. D., Lin, B., Lauvaux, T., O'dell, C., Meadows, B., Browell, E. V., Digangi, J. P., Sweeney, C.,
Mcgill, M. J., Barrick, J. D., Nehrir, A. R., Yang, M. M., Bennett, J. R., Baier, B. C., Roiger, A., Pal, S., Gerken, T., Fried,
A., Feng, S., Shrestha, R., Shook, M. A., Chen, G., Campbell, L. J., Barkley, Z. R., and Pauly, R. M.: ACT-America: L3
Merged In Situ Atmospheric Trace Gases and Flask Data, Eastern USA, ORNL DAAC,
https://doi.org/10.3334/ORNLDAAC/1593, 2018.

DiGangi, J. P., Choi, Y., Nowak, J. B., Halliday, H. S., Diskin, G. S., Feng, S., Barkley, Z. R., Lauvaux, T., Pal, S., Davis, K.
J., Baier, B. C., and Sweeney, C.: Seasonal Variability in Local Carbon Dioxide Biomass Burning Sources Over Central and
Eastern US Using Airborne In Situ Enhancement Ratios, Journal of Geophysical Research: Atmospheres, 126,
e2020JD034525, https://doi.org/10.1029/2020JD034525, 2021.

Díaz-Isaac, L. I., Lauvaux, T., and Davis, K. J.: Impact of physical parameterizations and initial conditions on simulated
atmospheric transport and CO₂ mole fractions in the US Midwest, Atmospheric Chemistry and
Physics Discussions, 1–40, https://doi.org/10.5194/acp-2018-117, 2018.

Draxler, R. R. and Hess, G. D.: Description of the HYSPLIT4 modeling system, 1997.

Feng, S., Lauvaux, T., Keller, K., Davis, K. J., Rayner, P., Oda, T., and Gurney, K. R.: A Road Map for Improving the
Treatment of Uncertainties in High-Resolution Regional Carbon Flux Inverse Estimates, Geophysical Research Letters, 46,
13461–13469, https://doi.org/10.1029/2019GL082987, 2019a.

Feng, S., Lauvaux, T., Davis, K. J., Keller, K., Zhou, Y., Williams, C., Schuh, A. E., Liu, J., and Baker, I.: Seasonal
Characteristics of Model Uncertainties From Biogenic Fluxes, Transport, and Large-Scale Boundary Inflow in Atmospheric
CO2 Simulations Over North America, Journal of Geophysical Research: Atmospheres, 124, 14325–14346,
https://doi.org/10.1029/2019JD031165, 2019b.

Feng, S., Lauvaux, T., Williams, C. A., Davis, K. J., Zhou, Y., Baker, I., Barkley, Z. R., and Wesloh, D.: Joint CO2 Mole
Fraction and Flux Analysis Confirms Missing Processes in CASA Terrestrial Carbon Uptake Over North America, Global
Biogeochemical Cycles, 35, e2020GB006914, https://doi.org/10.1029/2020GB006914, 2021a.

Feng, S., Lauvaux, T., Barkley, Z. R., Davis, K. J., Butler, M. P., Deng, A., Gaudet, B., and Stauffer, D.: ACT-America: WRF-Chem Baseline Simulations for North America, 2016-2019, ORNL DAAC, https://doi.org/10.3334/ORNLDAAC/1884, 2021b.

Fischer, M. L., Parazoo, N., Brophy, K., Cui, X., Jeong, S., Liu, J., Keeling, R., Taylor, T. E., Gurney, K., Oda, T., and Graven, H.: Simulating estimation of California fossil fuel and biosphere carbon dioxide exchanges combining in situ tower and satellite column observations, Journal of Geophysical Research: Atmospheres, 122, 3653–3671, https://doi.org/10.1002/2016JD025617, 2017.

Friedlingstein, P., O'Sullivan, M., Jones, M. W., Andrew, R. M., Gregor, L., Hauck, J., Le Quéré, C., Luijkx, I. T., Olsen, A., Peters, G. P., Peters, W., Pongratz, J., Schwingshackl, C., Sitch, S., Canadell, J. G., Ciais, P., Jackson, R. B., Alin, S. R., Alkama, R., Arneth, A., Arora, V. K., Bates, N. R., Becker, M., Bellouin, N., Bittig, H. C., Bopp, L., Chevallier, F., Chini, L. P., Cronin, M., Evans, W., Falk, S., Feely, R. A., Gasser, T., Gehlen, M., Gkritzalis, T., Gloege, L., Grassi, G., Gruber, N., Gürses, Ö., Harris, I., Hefner, M., Houghton, R. A., Hurtt, G. C., Iida, Y., Ilyina, T., Jain, A. K., Jersild, A., Kadono, K., Kato, E., Kennedy, D., Klein Goldewijk, K., Knauer, J., Korsbakken, J. I., Landschützer, P., Lefèvre, N., Lindsay, K., Liu, J., Liu, Z., Marland, G., Mayot, N., McGrath, M. J., Metzl, N., Monacci, N. M., Munro, D. R., Nakaoka, S.-I., Niwa, Y., O'Brien, K., Ono, T., Palmer, P. I., Pan, N., Pierrot, D., Pocock, K., Poulter, B., Resplandy, L., Robertson, E., Rödenbeck, C., Rodriguez, C., Rosan, T. M., Schwinger, J., Séférian, R., Shutler, J. D., Skjelvan, I., Steinhoff, T., Sun, Q., Sutton, A. J., Sweeney, C., Takao, S., Tanhua, T., Tans, P. P., Tian, X., Tian, H., Tilbrook, B., Tsujino, H., Tubiello, F., van der Werf, G. R., Walker, A. P., Wanninkhof, R., Whitehead, C., Willstrand Wranne, A., et al.: Global Carbon Budget 2022, Earth System Science Data, 14, 4811–4900, https://doi.org/10.5194/essd-14-4811-2022, 2022.

Gately, C. K. and Hutyra, L. R.: Large Uncertainties in Urban-Scale Carbon Emissions, Journal of Geophysical Research: Atmospheres, 122, 11,242-11,260, https://doi.org/10.1002/2017JD027359, 2017.

Gerken, T., Feng, S., Keller, K., Lauvaux, T., DiGangi, J. P., Choi, Y., Baier, B., and Davis, K. J.: Examining CO2 Model Observation Residuals Using ACT-America Data, Journal of Geophysical Research: Atmospheres, 126, e2020JD034481, https://doi.org/10.1029/2020JD034481, 2021.

Godwin, H.: Radiocarbon Dating: Fifth International Conference, Nature, 195, 943–945, https://doi.org/10.1038/195943a0, 1962.

Gonzalez, A., Millet, D. B., Yu, X., Wells, K. C., Griffis, T. J., Baier, B. C., Campbell, P. C., Choi, Y., DiGangi, J. P., Gvakharia, A., Halliday, H. S., Kort, E. A., McKain, K., Nowak, J. B., and Plant, G.: Fossil Versus Nonfossil CO Sources in the US: New Airborne Constraints From ACT-America and GEM, Geophysical Research Letters, 48, e2021GL093361, https://doi.org/10.1029/2021GL093361, 2021.

Graven, H. D., Guilderson, T. P., and Keeling, R. F.: Methods for High-Precision 14C AMS Measurement of Atmospheric CO2 at LLNL, Radiocarbon, 49, 349–356, https://doi.org/10.1017/S0033822200042284, 2007.

Graven, H. D., Stephens, B. B., Guilderson, T. P., Campos, T. L., Schimel, D. S., Campbell, J. E., and Keeling, R. F.: Vertical profiles of biospheric and fossil fuel-derived CO2 and fossil fuel CO2 :CO ratios from airborne measurements of Δ14C, CO2 and CO above Colorado, USA, Tellus B: Chemical and Physical Meteorology, 61, 536–546, https://doi.org/10.1111/j.1600-0889.2009.00421.x, 2009.

Formatted: Font: 10 pt

Formatted: Font: 10 pt, Font color: Text 1

Formatted: Font: 10 pt, No underline, Font color: Text 1

Formatted: Font: 10 pt, Font color: Text 1

Deleted: ¶

840 Graven, H. D. and Gruber, N.: Continental-scale enrichment of atmospheric $^{14}CO_2$ from the nuclear power industry: potential impact on the estimation of fossil fuel-derived CO_2, Atmospheric Chemistry and Physics, 11, 12339–12349, https://doi.org/10.5194/acp-11-12339-2011, 2011.

Graven, H., Fischer, M. L., Lueker, T., Jeong, S., Guilderson, T. P., Keeling, R. F., Bambha, R., Brophy, K., Callahan, W.,
845 Cui, X., Frankenberg, C., Gurney, K. R., LaFranchi, B. W., Lehman, S. J., Michelsen, H., Miller, J. B., Newman, S., Paplawsky, W., Parazoo, N. C., Sloop, C., and Walker, S. J.: Assessing fossil fuel CO2 emissions in California using atmospheric observations and models, Environ. Res. Lett., 13, 065007, https://doi.org/10.1088/1748-9326/aabd43, 2018.

Graven, H., Keeling, R. F., and Rogelj, J.: Changes to Carbon Isotopes in Atmospheric CO2 Over the Industrial Era and Into
850 the Future, Global Biogeochemical Cycles, 34, e2019GB006170, https://doi.org/10.1029/2019GB006170, 2020.

Gregg, J. S., Losey, L. M., Andres, R. J., Blasing, T. J., and Marland, G.: The Temporal and Spatial Distribution of Carbon Dioxide Emissions from Fossil-Fuel Use in North America, Journal of Applied Meteorology and Climatology, 48, 2528–2542, https://doi.org/10.1175/2009JAMC2115.1, 2009.
855

Gurney, K. R., Law, R. M., Denning, A. S., Rayner, P. J., Baker, D., Bousquet, P., Bruhwiler, L., Chen, Y.-H., Ciais, P., Fan, S., Fung, I. Y., Gloor, M., Heimann, M., Higuchi, K., John, J., Kowalczyk, E., Maki, T., Maksyutov, S., Peylin, P., Prather, M., Pak, B. C., Sarmiento, J., Taguchi, S., Takahashi, T., and Yuen, C.-W.: TransCom 3 CO2 inversion intercomparison: 1. Annual mean control results and sensitivity to transport and prior flux information, Tellus B, 55, 555–579,
860 https://doi.org/10.1034/j.1600-0889.2003.00049.x, 2003.

Gurney, K. R., Liang, J., Roest, G., Song, Y., Mueller, K., and Lauvaux, T.: Under-reporting of greenhouse gas emissions in U.S. cities, Nat Commun, 12, 553, https://doi.org/10.1038/s41467-020-20871-0, 2021.

865 Gurney, K. R., Liang, J., Patarasuk, R., Song, Y., Huang, J., and Roest, G.: The Vulcan Version 3.0 High-Resolution Fossil Fuel CO2 Emissions for the United States, Journal of Geophysical Research: Atmospheres, 125, e2020JD032974, https://doi.org/10.1029/2020JD032974, 2020.

Hayes, D. J., Turner, D. P., Stinson, G., McGuire, A. D., Wei, Y., West, T. O., Heath, L. S., de Jong, B., McConkey, B. G.,
870 Birdsey, R. A., Kurz, W. A., Jacobson, A. R., Huntzinger, D. N., Pan, Y., Post, W. M., and Cook, R. B.: Reconciling estimates of the contemporary North American carbon balance among terrestrial biosphere models, atmospheric inversions, and a new approach for estimating net ecosystem exchange from inventory-based data, Global Change Biology, 18, 1282–1299, https://doi.org/10.1111/j.1365-2486.2011.02627.x, 2012.

875 Hu, L., Montzka, S. A., Kaushik, A., Andrews, A. E., Sweeney, C., Miller, J., Baker, I. T., Denning, S., Campbell, E., Shiga, Y. P., Tans, P., Siso, M. C., Crotwell, M., McKain, K., Thoning, K., Hall, B., Vimont, I., Elkins, J. W., Whelan, M. E., and Suntharalingam, P.: COS-derived GPP relationships with temperature and light help explain high-latitude atmospheric CO2 seasonal cycle amplification, Proceedings of the National Academy of Sciences, 118, e2103423118, https://doi.org/10.1073/pnas.2103423118, 2021.
880

Jacobson, A. R., Schuldt, K. N., Miller, J. B., Oda, T., Tans, P., Arlyn Andrews, Mund, J., Ott, L., Collatz, G. J., Aalto, T., Afshar, S., Aikin, K., Aoki, S., Apadula, F., Baier, B., Bergamaschi, P., Beyersdorf, A., Biraud, S. C., Bollenbacher, A., Bowling, D., Brailsford, G., Abshire, J. B., Chen, G., Huilin Chen, Lukasz Chmura, Sites Climadat, Colomb, A., Conil, S., Cox, A., Cristofanelli, P., Cuevas, E., Curcoll, R., Sloop, C. D., Davis, K., Wekker, S. D., Delmotte, M., DiGangi, J. P.,
885 Dlugokencky, E., Ehleringer, J., Elkins, J. W., Emmenegger, L., Fischer, M. L., Forster, G., Frumau, A., Galkowski, M., Gatti, L. V., Gloor, E., Griffis, T., Hammer, S., Haszpra, L., Hatakka, J., Heliasz, M., Hensen, A., Hermanssen, O., Hintsa,

E., Holst, J., Jaffe, D., Karion, A., Kawa, S. R., Keeling, R., Keronen, P., Kolari, P., Kominkova, K., Kort, E., Krummel, P., Kubistin, D., Labuschagne, C., Langenfelds, R., Laurent, O., Laurila, T., Lauvaux, T., Law, B., Lee, J., Lehner, I., Leuenberger, M., Levin, I., Levula, J., Lin, J., Lindauer, M., Loh, Z., Lopez, M., Luijkx, I. T., Myhre, C. L., Machida, T., Mammarella, I., Manca, G., Manning, A., Manning, A., Marek, M. V., Marklund, P., Martin, M. Y., Matsueda, H., McKain, K., Meijer, H., Meinhardt, F., Miles, N., Miller, C. E., Mölder, M., Montzka, S., et al.: CarbonTracker CT2019B, https://doi.org/10.25925/20201008, 2020.

King, A. W., Dilling, L., Zimmerman, G. P., Fairman, D. M., Houghton, R. A., Marland, G., Rose, A. Z., and Wilbanks, T. J.: The first state of the carbon cycle report (SOCCR): The North American carbon budget and implications for the global carbon cycle., The first state of the carbon cycle report (SOCCR): The North American carbon budget and implications for the global carbon cycle., 2007.

King, A. W., Hayes, D. J., Huntzinger, D. N., West, T. O., and Post, W. M.: North American carbon dioxide sources and sinks: magnitude, attribution, and uncertainty, Frontiers in Ecology and the Environment, 10, 512–519, https://doi.org/10.1890/120066, 2015.

Kooijmans, L. M. J., Maseyk, K., Seibt, U., Sun, W., Vesala, T., Mammarella, I., Kolari, P., Aalto, J., Franchin, A., Vecchi, R., Valli, G., and Chen, H.: Canopy uptake dominates nighttime carbonyl sulfide fluxes in a boreal forest, Atmospheric Chemistry and Physics, 17, 11453–11465, https://doi.org/10.5194/acp-17-11453-2017, 2017.

Korff, S. A. and Mendell, R. B.: Variations in Radiocarbon Production in the Earth's Atmosphere, Radiocarbon, 22, 159–165, https://doi.org/10.1017/S0033822200009425, 1980.

Kuai, L., Parazoo, N. C., Shi, M., Miller, C. E., Baker, I., Bloom, A. A., Bowman, K., Lee, M., Zeng, Z.-C., Commane, R., Montzka, S. A., Berry, J., Sweeney, C., Miller, J. B., and Yung, Y. L.: Quantifying Northern High Latitude Gross Primary Productivity (GPP) Using Carbonyl Sulfide (OCS), Global Biogeochemical Cycles, 36, e2021GB007216, https://doi.org/10.1029/2021GB007216, 2022.

LaFranchi, B. W., Pétron, G., Miller, J. B., Lehman, S. J., Andrews, A. E., Dlugokencky, E. J., Hall, B., Miller, B. R., Montzka, S. A., Neff, W., Novelli, P. C., Sweeney, C., Turnbull, J. C., Wolfe, D. E., Tans, P. P., Gurney, K. R., and Guilderson, T. P.: Constraints on emissions of carbon monoxide, methane, and a suite of hydrocarbons in the Colorado Front Range using observations of ¹⁴CO₂, Atmospheric Chemistry and Physics, 13, 11101–11120, https://doi.org/10.5194/acp-13-11101-2013, 2013.

Lauvaux, T., Schuh, A. E., Uliasz, M., Richardson, S., Miles, N., Andrews, A. E., Sweeney, C., Diaz, L. I., Martins, D., Shepson, P. B., and Davis, K. J.: Constraining the CO2 budget of the corn belt: exploring uncertainties from the assumptions in a mesoscale inverse system, Atmos. Chem. Phys., 12, 337–354, https://doi.org/10.5194/acp-12-337-2012, 2012.

Lauvaux, T. and Davis, K. J.: Planetary boundary layer errors in mesoscale inversions of column-integrated CO2 measurements, Journal of Geophysical Research: Atmospheres, 119, 490–508, https://doi.org/10.1002/2013JD020175, 2014.

Lauvaux, T., Gurney, K. R., Miles, N. L., Davis, K. J., Richardson, S. J., Deng, A., Nathan, B. J., Oda, T., Wang, J. A., Hutyra, L., and Turnbull, J.: Policy-Relevant Assessment of Urban CO2 Emissions, Environ. Sci. Technol., 54, 10237–10245, https://doi.org/10.1021/acs.est.0c00343, 2020.

Lehman, S. J., Miller, J. B., Wolak, C., Southon, J., Tans, P. P., Montzka, S. A., Sweeney, C., Andrews, A., LaFranchi, B., Guilderson, T. P., and Turnbull, J. C.: Allocation of Terrestrial Carbon Sources Using 14CO2: Methods, Measurement, and Modeling, Radiocarbon, 55, 1484–1495, 2013.

Levin, I. and Karstens, U.: Inferring high-resolution fossil fuel CO2 records at continental sites from combined 14CO2 and CO observations, Tellus B: Chemical and Physical Meteorology, 59, 245–250, https://doi.org/10.1111/j.1600-0889.2006.00244.x, 2007.

Libby, W. F.: Atmospheric Helium Three and Radiocarbon from Cosmic Radiation, Phys. Rev., 69, 671–672, https://doi.org/10.1103/PhysRev.69.671.2, 1946.

Lin, J. C., Gerbig, C., Wofsy, S. C., Andrews, A. E., Daube, B. C., Davis, K. J., and Grainger, C. A.: A near-field tool for simulating the upstream influence of atmospheric observations: The Stochastic Time-Inverted Lagrangian Transport (STILT) model, J. Geophys. Res., 108, 4493, https://doi.org/10.1029/2002JD003161, 2003.

Lopez, M., Schmidt, M., Delmotte, M., Colomb, A., Gros, V., Janssen, C., Lehman, S. J., Mondelain, D., Perrussel, O., Ramonet, M., Xueref-Remy, I., and Bousquet, P.: CO, NO_x and $^{13}CO_2$ as tracers for fossil fuel CO_2: results from a pilot study in Paris during winter 2010, Atmospheric Chemistry and Physics, 13, 7343–7358, https://doi.org/10.5194/acp-13-7343-2013, 2013.

Ma, J., Remaud, M., Peylin, P., Patra, P., Niwa, Y., Rodenbeck, C., Cartwright, M., Harrison, J. J., Chipperfield, M. P., Pope, R. J., Wilson, C., Belviso, S., Montzka, S. A., Vimont, I., Moore, F., Atlas, E. L., Schwartz, E., and Krol, M. C.: Intercomparison of Atmospheric Carbonyl Sulfide (TransCom-COS): 2. Evaluation of Optimized Fluxes Using Ground-Based and Aircraft Observations, Journal of Geophysical Research: Atmospheres, 128, e2023JD039198, https://doi.org/10.1029/2023JD039198, 2023.

Maier, F., Rödenbeck, C., Levin, I., Gerbig, C., Gachkivskyi, M., and Hammer, S.: Potential of 14C-based vs. ΔCO-based ΔffCO$_2$ observations to estimate urban fossil fuel CO$_2$ (ffCO$_2$) emissions, Atmos. Chem. Phys., 24, 8183-8203, http://doi.org/10.5914/acp-24-8183-2024, 2024a.

Maier, F., Levin, I., Conil, S., Gachkivskyi, M., Denier van der Gon, H., and Hammer, S.: Uncertainty in continuous ΔCO-based ΔffCO$_2$ estimates derived from ^{14}C flask and bottom-up ΔCO/ΔffCO$_2$ ratios, Atmos. Chem. Phys., 24, 8205–8223, https://doi.org/10.5194/acp-24-8205-2024, 2024b.

Miles, N. L., Richardson, S. J., Davis, K. J., Lauvaux, T., Andrews, A. E., West, T. O., Bandaru, V., and Crosson, E. R.: Large amplitude spatial and temporal gradients in atmospheric boundary layer CO2 mole fractions detected with a tower-based network in the U.S. upper Midwest, Journal of Geophysical Research: Biogeosciences, 117, https://doi.org/10.1029/2011JG001781, 2012.

Miller, J. B., Lehman, S. J., Montzka, S. A., Sweeney, C., Miller, B. R., Karion, A., Wolak, C., Dlugokencky, E. J., Southon, J., Turnbull, J. C., and Tans, P. P.: Linking emissions of fossil fuel CO2 and other anthropogenic trace gases using atmospheric 14CO2, Journal of Geophysical Research: Atmospheres, 117, https://doi.org/10.1029/2011JD017048, 2012.

Miller, J. B., Lehman, S. J., Verhulst, K. R., Miller, C. E., Duren, R. M., Yadav, V., Newman, S., and Sloop, C. D.: Large and seasonally varying biospheric CO2 fluxes in the Los Angeles megacity revealed by atmospheric radiocarbon, PNAS, 117, 26681–26687, https://doi.org/10.1073/pnas.2005253117, 2020.

Montzka, S. A., Calvert, P., Hall, B. D., Elkins, J. W., Conway, T. J., Tans, P. P., and Sweeney, C.: On the global distribution, seasonality, and budget of atmospheric carbonyl sulfide (COS) and some similarities to CO2, Journal of Geophysical Research: Atmospheres, 112, https://doi.org/10.1029/2006JD007665, 2007.

990

Oda, T., Maksyutov, S., and Andres, R. J.: The Open-source Data Inventory for Anthropogenic CO_2, version 2016 (ODIAC2016): a global monthly fossil fuel CO_2 gridded emissions data product for tracer transport simulations and surface flux inversions, Earth System Science Data, 10, 87–107, https://doi.org/10.5194/essd-10-87-2018, 2018.

995

Pal, S., Davis, K. J., Lauvaux, T., Browell, E. V., Gaudet, B. J., Stauffer, D. R., Obland, M. D., Choi, Y., DiGangi, J. P., Feng, S., Lin, B., Miles, N. L., Pauly, R. M., Richardson, S. J., and Zhang, F.: Observations of Greenhouse Gas Changes Across Summer Frontal Boundaries in the Eastern United States, Journal of Geophysical Research: Atmospheres, 125, e2019JD030526, https://doi.org/10.1029/2019JD030526, 2020.

1000

Parazoo, N. C., Bowman, K. W., Baier, B. C., Liu, J., Lee, M., Kuai, L., Shiga, Y., Baker, I., Whelan, M. E., Feng, S., Krol, M., Sweeney, C., Runkle, B. R., Tajfar, E., and Davis, K. J.: Covariation of Airborne Biogenic Tracers (CO2, COS, and CO) Supports Stronger Than Expected Growing Season Photosynthetic Uptake in the Southeastern US, Global Biogeochemical Cycles, 35, e2021GB006956, https://doi.org/10.1029/2021GB006956, 2021.

1005

Peylin, P., Law, R. M., Gurney, K. R., Chevallier, F., Jacobson, A. R., Maki, T., Niwa, Y., Patra, P. K., Peters, W., and Rayner, P. J.: Global atmospheric carbon budget: results from an ensemble of atmospheric CO2 inversions, Biogeosciences, 10, 6699–6720, 2013.

Potosnak, M. J., Wofsy, S. C., Denning, A. S., Conway, T. J., Munger, J. W., and Barnes, D. H.: Influence of biotic exchange and combustion sources on atmospheric CO2 concentrations in New England from observations at a forest flux tower, Journal of Geophysical Research: Atmospheres, 104, 9561–9569, https://doi.org/10.1029/1999JD900102, 1999.

1010

Schuh, A. E., Denning, A. S., Corbin, K. D., Baker, I. T., Uliasz, M., Parazoo, N., Andrews, A. E., and Worthy, D. E. J.: A regional high-resolution carbon flux inversion of North America for 2004, Biogeosciences, 7, 1625–1644, https://doi.org/10.5194/bg-7-1625-2010, 2010.

1015

Shiga, Y. P., Michalak, A. M., Gourdji, S. M., Mueller, K. L., and Yadav, V.: Detecting fossil fuel emissions patterns from subcontinental regions using North American in situ CO2 measurements, Geophysical Research Letters, 41, 4381–4388, https://doi.org/10.1002/2014GL059684, 2014.

1020

Stephens, B. B., Gurney, K. R., Tans, P. P., Sweeney, C., Peters, W., Bruhwiler, L., Ciais, P., Ramonet, M., Bousquet, P., Nakazawa, T., Aoki, S., Machida, T., Inoue, G., Vinnichenko, N., Lloyd, J., Jordan, A., Heimann, M., Shibistova, O., Langenfelds, R. L., Steele, L. P., Francey, R. J., and Denning, A. S.: Weak Northern and Strong Tropical Land Carbon Uptake from Vertical Profiles of Atmospheric CO2, Science, 316, 1732–1735, https://doi.org/10.1126/science.1137004, 2007.

1025

Stuiver, M. and Polach, H. A.: Discussion Reporting of 14C Data, Radiocarbon, 19, 355–363, https://doi.org/10.1017/S0033822200003672, 1977.

Sun, W., Maseyk, K., Lett, C., and Seibt, U.: Litter dominates surface fluxes of carbonyl sulfide in a Californian oak woodland, Journal of Geophysical Research: Biogeosciences, 121, 438–450, https://doi.org/10.1002/2015JG003149, 2016.

1040 Tans, P. P., Fung, I. Y., and Takahashi, T.: Observational contrains on the global atmospheric co2 budget, Science, 247, 1431–1438, https://doi.org/10.1126/science.247.4949.1431, 1990.

Tans, P. P., Berry, J. A., and Keeling, R. F.: Oceanic 13C/12C observations: A new window on ocean CO2 uptake, Global Biogeochem. Cycles, 7, 353–368, https://doi.org/10.1029/93GB00053, 1993.

1045 Thompson, M. V. and Randerson, J. T.: Impulse response functions of terrestrial carbon cycle models: method and application, Global Change Biology, 5, 371–394, https://doi.org/10.1046/j.1365-2486.1999.00235.x, 1999.

Turnbull, J. C., Miller, J. B., Lehman, S. J., Tans, P. P., Sparks, R. J., and Southon, J.: Comparison of 14CO2, CO, and SF6 as tracers for recently added fossil fuel CO2 in the atmosphere and implications for biological CO2 exchange, Geophys. Res. 1050 Lett., 33, L01817, https://doi.org/10.1029/2005GL024213, 2006.

Turnbull, J. C., Lehman, S. J., Miller, J. B., Sparks, R. J., Southon, J. R., and Tans, P. P.: A new high precision 14CO2 time series for North American continental air, Journal of Geophysical Research: Atmospheres, 112, https://doi.org/10.1029/2006JD008184, 2007.

1055

Turnbull, J., Rayner, P., Miller, J., Naegler, T., Ciais, P., and Cozic, A.: On the use of 14CO2 as a tracer for fossil fuel CO2: Quantifying uncertainties using an atmospheric transport model, J. Geophys. Res., 114, D22302, https://doi.org/10.1029/2009JD012308, 2009.

1060 Turnbull, J. C., Karion, A., Fischer, M. L., Faloona, I., Guilderson, T., Lehman, S. J., Miller, B. R., Miller, J. B., Montzka, S., Sherwood, T., Saripalli, S., Sweeney, C., and Tans, P. P.: Assessment of fossil fuel carbon dioxide and other anthropogenic trace gas emissions from airborne measurements over Sacramento, California in spring 2009, Atmos. Chem. Phys., 11, 705–721, https://doi.org/10.5194/acp-11-705-2011, 2011a.

1065 Turnbull, J. C., Tans, P. P., Lehman, S. J., Baker, D., Conway, T. J., Chung, Y. S., Gregg, J., Miller, J. B., Southon, J. R., and Zhou, L.-X.: Atmospheric observations of carbon monoxide and fossil fuel CO2 emissions from East Asia, J. Geophys. Res., 116, D24306, https://doi.org/10.1029/2011JD016691, 2011b.

Turnbull, J. C., Sweeney, C., Karion, A., Newberger, T., Lehman, S. J., Tans, P. P., Davis, K. J., Lauvaux, T., Miles, N. L., 1070 Richardson, S. J., Cambaliza, M. O., Shepson, P. B., Gurney, K., Patarasuk, R., and Razlivanov, I.: Toward quantification and source sector identification of fossil fuel CO2 emissions from an urban area: Results from the INFLUX experiment, J. Geophys. Res. Atmos., 120, 2014JD022555, https://doi.org/10.1002/2014JD022555, 2015.

Turnbull, J. C., Karion, A., Davis, K. J., Lauvaux, T., Miles, N. L., Richardson, S. J., Sweeney, C., McKain, K., Lehman, S. 1075 J., Gurney, K. R., Patarasuk, R., Liang, J., Shepson, P. B., Heimburger, A., Harvey, R., and Whetstone, J.: Synthesis of Urban CO2 Emission Estimates from Multiple Methods from the Indianapolis Flux Project (INFLUX), Environ. Sci. Technol., 53, 287–295, https://doi.org/10.1021/acs.est.8b05552, 2019.

USGCRP: Second State of the Carbon Cycle Report, U.S. Global Change Research Program, Washington, DC, 2018.
1080

Vaughn, B. H., Miller, J., Ferretti, D. F., and White, J. W. C.: Stable isotope measurements of atmospheric CO2 and CH4, in: Handbook of Stable Isotope Analytical Techniques, Elsevier, 272–304, 2004.

Vimont, I. J., Turnbull, J. C., Petrenko, V. V., Place, P. F., Karion, A., Miles, N. L., Richardson, S. J., Gurney, K., Patarasuk, R., Sweeney, C., Vaughn, B., and White, J. W. C.: Carbon monoxide isotopic measurements in Indianapolis constrain urban source isotopic signatures and support mobile fossil fuel emissions as the dominant wintertime CO source, Elementa: Science of the Anthropocene, 5, 63, https://doi.org/10.1525/elementa.136, 2017.

Vogel, F., Hamme, S., Steinhof, A., Kromer, B., and Levin, I.: Implication of weekly and diurnal 14C calibration on hourly estimates of CO-based fossil fuel CO2 ata moderately polluted site in southwestern Germany, Tellus B: Chemical and Physical Meteorology, 62, 512–520, https://doi.org/10.1111/j.1600-0889.2010.00477.x, 2010.

Whelan, M. E., Shi, M., Sun, W., Vries, L. K., Seibt, U., and Maseyk, K.: Soil Carbonyl Sulfide (OCS) Fluxes in Terrestrial Ecosystems: An Empirical Model, Journal of Geophysical Research: Biogeosciences, 127, e2022JG006858, https://doi.org/10.1029/2022JG006858, 2022.

Wei, Y., Shrestha, R., Pal, S., Gerken, T., Feng, S., McNelis, J., Singh, D., Thornton, M. M., Boyer, A. G., Shook, M. A., Chen, G., Baier, B. C., Barkley, Z. R., Barrick, J. D., Bennett, J. R., Browell, E. V., Campbell, J. F., Campbell, L. J., Choi, Y., Collins, J., Dobler, J., Eckl, M., Fiehn, A., Fried, A., Digangi, J. P., Barton-Grimley, R., Halliday, H., Klausner, T., Kooi, S., Kostinek, J., Lauvaux, T., Lin, B., McGill, M. J., Meadows, B., Miles, N. L., Nehrir, A. R., Nowak, J. B., Obland, M., O'Dell, C., Fao, R. M. P., Richardson, S. J., Richter, D., Roiger, A., Sweeney, C., Walega, J., Weibring, P., Williams, C. A., Yang, M. M., Zhou, Y., and Davis, K. J.: Atmospheric Carbon and Transport – America (ACT-America) Data Sets: Description, Management, and Delivery, Earth and Space Science, 8, e2020EA001634, https://doi.org/10.1029/2020EA001634, 2021.

Wu, K., Davis, K. J., Miles, N. L., Richardson, S. J., Lauvaux, T., Sarmiento, D. P., Balashov, N. V., Keller, K., Turnbull, J., Gurney, K. R., Liang, J., and Roest, G.: Source decomposition of eddy-covariance CO2 flux measurements for evaluating a high-resolution urban CO2 emissions inventory, Environ. Res. Lett., 17, 074035, https://doi.org/10.1088/1748-9326/ac7c29, 2022.

Zazzeri, G., Graven, H., Xu, X., Saboya, E., Blyth, L., Manning, A. J., Chawner, H., Wu, D., and Hammer, S.: Radiocarbon Measurements Reveal Underestimated Fossil CH4 and CO2 Emissions in London, Geophysical Research Letters, 50, e2023GL103834, https://doi.org/10.1029/2023GL103834, 2023.

Zhou, Y., Williams, C. A., Lauvaux, T., Davis, K. J., Feng, S., Baker, I., Denning, S., and Wei, Y.: A Multiyear Gridded Data Ensemble of Surface Biogenic Carbon Fluxes for North America: Evaluation and Analysis of Results, Journal of Geophysical Research: Biogeosciences, 125, e2019JG005314, https://doi.org/10.1029/2019JG005314, 2020.